

Review

Design principles for 2D transition metal dichalcogenides toward lithium–sulfur batteries

Xiaoyu Yu,^{1,2} Yifan Ding,^{1,2} and Jingyu Sun^{1,*}

SUMMARY

Lithium–sulfur (Li–S) batteries are regarded as a promising candidate for next-generation energy storage systems owing to their remarkable energy density, resource availability, and environmental benignity. Nevertheless, severe shuttling effect, sluggish redox kinetics, large volumetric expansion, and uncontrollable dendrite growth hamper the practical applications. To address these intractable issues, two-dimensional (2D) transition metal dichalcogenides (TMDs) have emerged expeditiously as an essential material strategy. Herein, this review emphasizes the development and application of 2D TMDs in Li–S batteries. It starts with introducing the fundamentals of Li–S batteries and common synthetic routes of TMDs, followed by summarizing the employment of pristine, hybrid, and defective TMDs in the realm of expediting sulfur chemistry and stabilizing lithium anode. Finally, the development roadmap and possible research directions of TMDs are proposed to offer guidance for the future design of high-performance Li–S batteries.

INTRODUCTION

Increasing demand for portable electronic devices has significantly accelerated the development of high-energy-density batteries. Nevertheless, commercial lithium-ion batteries have almost approached their theoretical energy density. Therefore, it is urgent to develop alternative energy storage systems with superior energy density and better economical effectiveness.^{1,2} Of note, lithium–sulfur (Li–S) battery is regarded as one of the most promising substitutes for its remarkable theoretical capacity (1672 mAh g⁻¹) and energy density (2600 Wh kg⁻¹), as well as the cost-effectiveness and environmental-friendliness of sulfur resource.^{3–5} However, the practicability of Li–S battery is plagued by several challenges^{6–8}: 1) The insulating nature of sulfur and its final discharge species Li₂S/Li₂S₂ cause the large electrochemical polarization and sluggish redox kinetics. 2) The large density difference between sulfur and Li₂S/Li₂S₂ leads to marked volumetric expansion. 3) The soluble long-chain polysulfides in liquid electrolyte react with metallic lithium because of the shuttle effect between the sulfur cathode and lithium anode, which results in a low Coulombic efficiency and active material loss. 4) The inhomogeneity of electrical field triggers uncontrollable dendrite growth. 5) On account of the infinite volume change during lithium plating and stripping process, solid electrolyte interface (SEI) layer repeated ruptures.

To address these intractable issues pertaining to Li–S batteries, two-dimensional (2D) materials have been utilized for their intriguing feature, including graphene,⁹ hexagonal boron nitride,¹⁰ MXene,¹¹ and transition metal dichalcogenides.¹² Among them, transition metal dichalcogenides (TMDs) have triggered great interest in recent years as a promising branch. In contrast to other 2D carbon-based materials, TMDs provide abundant polar sites favorable for the chemical adsorption of lithium polysulfides (LiPSs). Therefore, combined with the highly active electrocatalytic ability, TMDs have been demonstrated to be a promising candidate to inhibit shuttle effect in Li–S batteries.^{13,14} Simultaneously, TMDs also play a key role in the modification of lithium anode because of the layered structure and lithiophilic property.¹⁵ Hence, understanding the key role of various TMDs as well as the design principles toward high-energy-density Li–S batteries is of great importance for future development.

In this review, we elaborate on the current advances and future directions of TMDs toward high-performance Li–S batteries. To begin with, the fundamentals of Li–S batteries and the properties of TMDs are introduced in detail. Then, we summarize the recent progress on the synthesis of different TMDs with an emphasis on the merit and demerit. Subsequently, we highlighted the application of TMDs in Li–S

¹College of Energy, Soochow Institute for Energy and Materials Innovations, Key Laboratory of Advanced Carbon Materials and Wearable Energy Technologies of Jiangsu Province, Soochow University, Suzhou 215006, P.R.China

²These authors contributed equally to this work.

*Correspondence: sunjy86@suda.edu.cn
<https://doi.org/10.1016/j.isci.2023.107489>



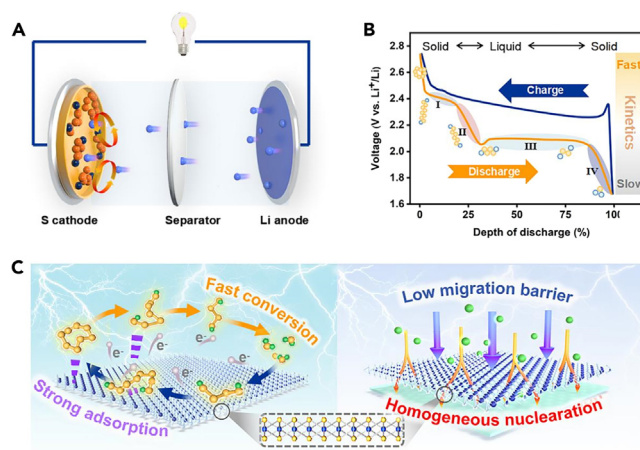


Figure 1. Schematic representation, voltage profiles, and mechanism illustration

(A) Schematic representation of a Li-S battery.

(B) Typical charge/discharge voltage profile of Li-S batteries and corresponding intermediate and product.

(C) Illustration of the mechanism of TMDs in sulfur chemistry and lithium anode.

batteries, including in the sulfur cathode and lithium anode. Finally, the concluding section presents the challenges and perspectives of this fast-growing realm. By reviewing all these, it is anticipated that the synthesis-structure-function relationship between the TMDs and Li-S chemistry is clarified to offer profound guidance for the future design of high-performance Li-S batteries.

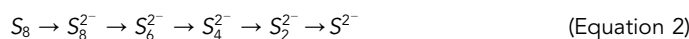
FUNDAMENTALS

Working mechanism of Li-S batteries

As demonstrated in Figure 1A, a conventional Li-S battery is composed of lithium metal anode, organic liquid electrolyte, and sulfur composite cathode. Generally speaking, it operates on a 16-electron conversion, which contributes to a superior theoretical capacity (1672 mAh g^{-1})¹⁶:



Figure 1B reveals the charge and discharge voltage profile of a typical Li-S battery. During the discharge process (the yellow curve), sulfur reacts with the lithium ions, undergoing reduction in a stepwise manner to ultimately form insoluble lithium sulfide.



Specifically, in stages I and II, the pristine S_8 molecule first reacts with the Li^+ to form a series of long-chain LiPSs (Li_2S_x , $4 \leq x \leq 8$). The top voltage plateau serves as a presentation of this process, which contributes to 25% of the theoretical capacity of sulfur (418 mAh g^{-1}).¹⁷ Unfortunately, long-chain LiPSs which readily dissolve into the electrolyte can migrate to anode and react with metallic lithium (instead of Li^+ and e^-). This inevitable shuttle effect leads to severe self-discharge and low Coulombic efficiency.

In stage III, these LiPSs further lithiated by a liquid-solid transformation process to the insoluble $\text{Li}_2\text{S}_2/\text{Li}_2\text{S}$ species. This is represented by the lower voltage plateau, which contributes to a higher theoretical capacity of about 1254 mAh g^{-1} (75% of the theoretical capacity of active sulfur species).¹⁸ On the basis of previous experimental results and theoretical analysis, this liquid-solid transition exhibits a much higher activation barrier than the previous steps, thus resulting to gradually decreased redox kinetics.^{19,20}

Stage IV describes the final stage as the further reduction of Li_2S_2 to Li_2S , which suffers strong polarization and sluggish kinetics as a result of the solid-solid transition reaction.

On the lithium anode side, lithium ions and electrons are produced when the lithium metal is oxidized, and migrate in the electrolyte to react with the sulfur cathode:



Unfortunately, the anode-electrolyte interface experiences uneven Li^+ flow and results in uncontrollable dendrite formation. Even worse, the SEI is usually inhomogeneous causing continuous side reactions between lithium anode and electrolyte.

Concerning the reversible charging process, the opposite pathway occurs, which matches the blue curve in Figure 1B.

Properties of 2D TMDs in Li–S batteries

2D TMDs have sparked considerable interest in the Li–S realm for their various chemical composition, tunable band structures, and distinctive electronic structures that differ themselves from other 2D materials and their bulk counterparts.²¹

As shown in Figure 1C, each monolayer of TMDs is made up of a “X–M–X” (M = transition metal elements from group IVB to group VIII; X = S, Se, Te) sandwich structure with three atom layers. These stacked layers of TMDs materials are readily to be isolated because of the weak van der Waals forces of atom layers. In terms of Li–S batteries, the unique structure endows TMDs with strong polarity, which can efficiently reinforce LiPS adsorption in contrast to bare carbon.^{22,23} Furthermore, 2D TMDs exhibit a large specific surface area and low migration energy barriers, consequently allowing the fast intercalation and deintercalation of Li^+ .²⁴ Notably, unlike other inactive materials, when employed in sulfur cathode, TMD is able to react with Li^+ and contributes extra capacity within the same working window as S_8 (1.7–2.8 V).²⁵ In the presence of lithiated TMD, the suppression of the shuttling effect is even more obvious, thus improving the cycling stability.²⁶

Distinguished by the stacking order of atomic planes (X–M–X), there are three kinds of well-known polytypic structures widely studied in Li–S batteries, namely 1T (octahedral), 2H (trigonal prismatic), and 1T' (distorted octahedral). Electronic characteristics vary depending on the diversity of structural phases. For instance, the metallic 1T phase of MoS_2 possessing high electrical conductivity of $10\text{--}100\text{ S cm}^{-1}$ is almost 10^7 times more conductive than its semiconducting 2H phase.²⁷ More interestingly, TMDs can transition from an indirect band gap semiconductor to a direct band gap semiconductor when the thickness is reduced.²⁸ This endows it with the role of ideal conductive material like graphene for Li–S batteries.

Moreover, the unsaturated heteroatom along with synergistic metal *d*-orbitals offers TMDs an effective *d*-band structure with catalytic properties.^{29,30} According to the *d*-band center theory, metal site with a higher *d*-band center exhibits stronger affinity to adsorbates. As for TMDs, raised *d*-band of metal sites is beneficial to further strengthen the interaction between polysulfides and catalysts for the lower reaction barrier.^{20,31} Notably, the electronic structure of TMDs can be tuned by some emerging strategies, including hybrid engineering and defective engineering.^{32,33}

Consequently, these obvious merits render 2D TMDs possible applications in high-performance Li–S batteries.

SYNTHESIS OF TMDs

Since the stripping of graphene in 2004, we have witnessed explosive growth regarding the application of 2D TMDs with a similar structure in electrochemical energy storage (EES) devices. The rational synthesis method of TMDs can be divided into two categories: top-down exfoliation³⁴ and bottom-up synthesis.^{28,35} In this section, we will introduce and discuss the three most widely used synthetic routes of TMDs in EES devices with emphasis on the advantages and disadvantages of each method in five aspects, including product quality, purity, yield, scalability, and cost-effectiveness (Figures 2A–C).

Liquid exfoliation

The sandwich-like MX_2 structure linked by weak van der Waals forces is readily to be isolated, which makes solution exfoliation a possible way to produce 2D TMDs.³⁷ Generally, direct sonication of layered TMDs in suitable solvents contributes to enlarging the interlayer space and weakening the interlayer connection (Figure 2D).³⁶ In this case, 2D MoS_2 , WS_2 , MoSe_2 , NbSe_2 , TaSe_2 , and MoTe_2 nanosheets have been prepared by this way.^{38–40} Owing to their simple operation stages, low prices, and solution processability, liquid exfoliation has good commercial prospects. However, it is hampered by limited yield and purity of the product.

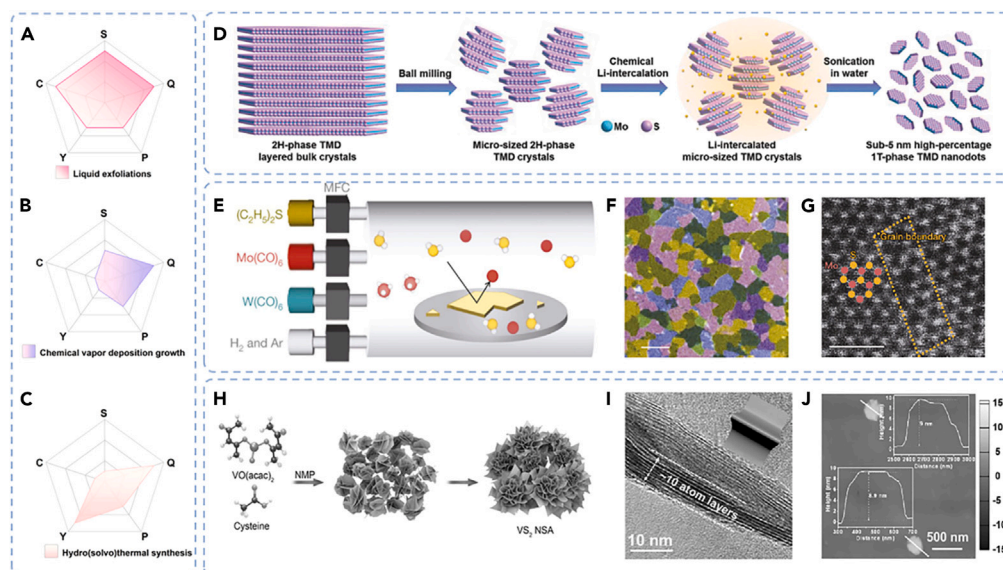


Figure 2. Typical synthesis of TMDs and comparison of each synthesis

(A–C) Evaluation on (A) liquid exfoliation, (B) CVD growth, and (C) Hydro(solvo)thermal synthesis in five aspects including product quality (Q), purity (P), yield (Y), scalability (S), and cost-effectiveness (C).

(D) Schematic of the synthetic procedure of 1T-phase, single-layer TMD nanodots by Li-intercalation liquid exfoliation.³⁶ Copyright 2018, Wiley-VCH.

(E) Schematic of the MOCVD process.

(F and G) False-color DF-TEM image and (G) ADF-STEM image of a continuous monolayer MoS₂ film. Scale bars: (F) 1 μm and (G) 1 nm.²⁸ Copyright 2015, Nature Publishing Group.

(H) Schematic of VS₂ nanosheet assembled by a solvothermal method.

(I) TEM image of VS₂ nanosheet assemblies.

(J) AFM image of individual nanosheets.³⁵ Copyright 2017, Wiley-VCH.

CVD growth

Chemical vapor deposition (CVD) growth is a typical bottom-up synthesis routine. The products possess the advantage of high quality and precisely controlled layer numbers.^{41–43} Moreover, Kang et al. have proved that metal-organic CVD based on gas-phase precursors readily achieved large-scale growth of 2D TMDs (Figures 2E–G).²⁸ Nevertheless, CVD growth is plagued by rigorous reaction conditions (high temperature and high vacuum).

Hydro(solvo)thermal synthesis

Compared with CVD growth, hydro(solvo)thermal synthesis is simpler and safer to operate as another famous bottom-up strategy.⁴⁴ Under the condition of hydrothermal or solvothermal, M and X species tend to accumulate to form MX₂ and grow into 2D nanosheets (Figures 2H–J).³⁵ However, the product quality is sensitive to temperature, time, and other reaction conditions. Furthermore, the architecture varies, such as spheres, flowers, boxes, and tubes, and it is difficult to obtain single-layer TMDS by adjusting these parameters.^{45–47}

APPLICATION OF TMDs IN SULFUR CHEMISTRY

Pristine TMDs

To the best of our knowledge, the LiPSs shuttle effect is undeniably the primary cause of the poor performance in Li–S batteries.^{48,49} In general, enhancing the adsorption of LiPSs and promoting the conversion to Li₂S are effective methods to solve this problem. To date, considerable progress on porous carbon materials to restrict the shuttle effect has been achieved, such as graphene, carbon nanotube (CNT), and hollow carbon spheres.^{50–52}

However, the weak physical confinement between nonpolar carbon materials and polar LiPSs inevitably leads to poor adsorption and eventually leads to unsatisfactory performance.⁵³ In this connection, polar

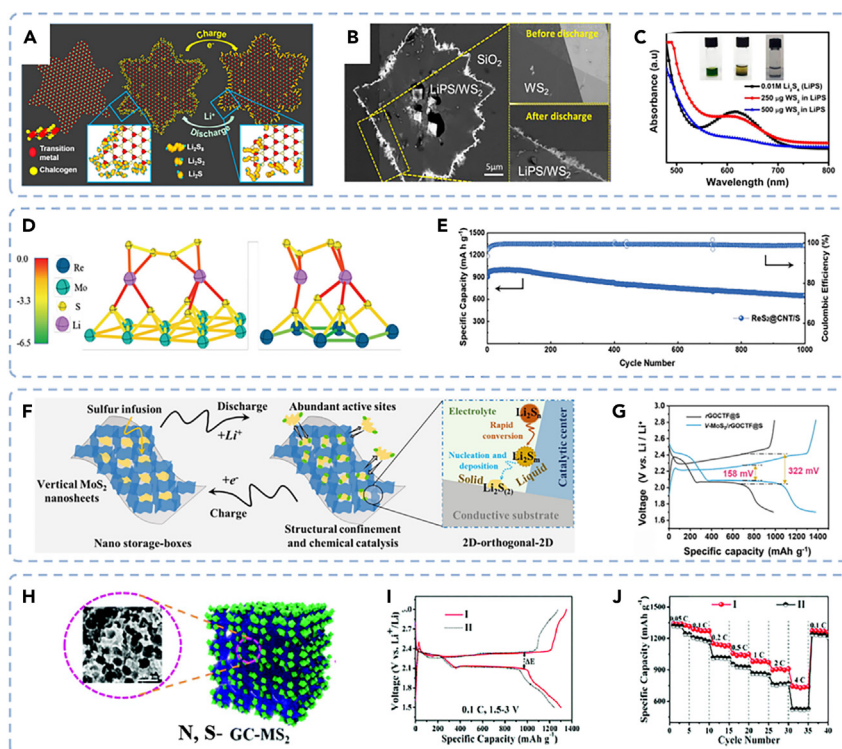


Figure 3. Pristine TMDs and carbon-supported TMDs in sulfur chemistry

- (A) Schematic of preferential adsorption sites for LiPSs of TMDs and their conversion during discharge-charge processes.
 (B) SEM image of short-chain LiPS confinement at catalytic edge sites of WS₂ nanosheets during discharge process.
 (C) UV-vis spectra of LiPS showing variation in color upon adsorption on WS₂ nanosheets.²⁹ Copyright 2016, American Chemical Society.
 (D) Crystal orbital Hamilton population analyses for Li₂S₄@MoS₂ and Li₂S₄@ReS₂ after relaxation.
 (E) Long-term cycling performance of Li-S cells with the ReS₂@CNT/S cathode at 1C.⁵⁵ Copyright 2020, Wiley-VCH.
 (F) Schematic of mechanisms of V-MoS₂/rGOCTF//LE//Li cell.
 (G) Charge/discharge profiles of rGOCTF@S//LE//Li and V-MoS₂/rGOCTF@S//LE//Li cells.⁵⁶ Copyright 2022, ELSEVIER B.V.
 (H) Schematic of the N, S-co-doped porous carbon-MS₂.
 (I) The first galvanostatic charge-discharge profiles of the different mass ratios of GC and CoS₂.
 (J) Rate performance of (I) GC-CoS₂/S and (II) GC-NiS₂/S cathodes.⁵⁷ Copyright 2020, The Royal Society of Chemistry.

TMDs show great potential in immobilizing LiPSs by chemical confinement. Besides, some of these materials display comparable conductivity but much higher electrocatalytic activity and electrochemical stability than carbon materials. To this end, transition metal dichalcogenide shows evidently proof to stabilize Li-S batteries by restraining shuttle effect.⁵⁴ With a combination of spectroscopic and microscopic analysis techniques, Babu et al. revealed the preferential adsorption of higher-order liquid polysulfides at the edge sites, which also serve as catalytic center (Figure 3A–C).²⁹

TMDs composites

Carbon-supported TMDs

Although considerable progress has been made regarding pristine TMDs as efficient cathode material in Li-S batteries, their further application is still impeded because of insufficient catalytic active sites and limited conductivity. Consequently, carbon materials have been introduced to TMDs to further optimize their performance in Li-S batteries, including graphene,⁵⁸ CNT,⁵⁹ heteroatom-doped carbon,⁶⁰ and other carbon-based materials.⁶¹

Rhenium disulfide (ReS₂), a novel member of the TMDs family, exhibits a number of unique properties as well as remarkable electrocatalytic activity.⁶² Taking Li₂S₄ as LiPSs guest model on surface of the MoS₂

and ReS₂, He et al. utilized crystal orbital Hamilton population analyses to quantify the nature and strength of the orbital overlap between different atoms (Figure 3D).⁵⁵ Despite the similar bonding orbital overlaps between Mo–S and Re–S atoms, the Re atoms establish a distinguished stronger bonding pattern as compared to the Mo atoms. In this regard, the designed nanocomposite of 1T'-phase 2D ReS₂ nanosheets *in situ* grown on the 1D carbon nanotubes (ReS₂@CNT) manifests abundant active sites which provide a high catalytic activity for efficient LiPSs conversion. As illustrated in Figure 3E, the obtained ReS₂@CNT cathode exhibits superb electrochemical cycle stability with a retention of 71.7% over 1000 cycles even at a high current density of 1 C (1675 mA g⁻¹).

It is worth noting that the effective combination of structural constraints and chemical catalysis can make the most difference through proper design.⁶³ Cui et al. constructed a self-supporting sulfur cathode with a nano-storage-box structure, in which V-MoS₂ serves as the wall and rGO as the bottom (Figure 3F).⁵⁶ The exposed edge active sites of V-MoS₂ are maximized by the 2D-orthogonal-2D structure. Furthermore, V-MoS₂ in conjunction with the conductive substrate forms a nano-storage-box that promotes the uniform dispersion of active materials. This synergistic effect of catalytic V-MoS₂ and conductive rGO successfully improves the performance of Li–S batteries (Figure 3G). Similarly, Zhang et al. designed a high conductive frame that possesses dual anchoring effect of physical confinement from porous structure and chemical entrapment of half-metallic CoS₂. Thus, the integrated cathode manifests an enhanced performance.⁶⁴

However, nonpolar carbon in general is not adequate for LiPSs confinement, limiting the overall adsorption effect of the material. Special attention has been paid to heteroatom-doped carbon,⁶⁵ which can not only provide adequate adsorption/containment but also enhances catalytic conversion of LiPSs. For instance, a nitrogen-doped CNT/graphene heterostructure was modified as a scaffold to accommodate sulfur in Li–S battery.⁶⁶ Due to the incorporation of N atoms, the carbon framework is endowed with more defects and active sites, resulting in advanced interfacial adsorption and superior electrochemical behavior. Density functional theory (DFT) calculation and reliable experimental results indicate that advanced doping strategies for carbon materials, such as introducing B, S, and P, can also visibly enhance the chemical interaction between LiPSs and carbon materials.⁶⁷ To this end, Liu et al. constructed a biomass-derived N, S-co-doped hierarchical porous carbon with MS₂ (M = Co, Ni), serving as a hybrid 3D sulfur host (Figure 3H).⁵⁷ Through such a unique structure, the electron transfer for conversion reactions is significantly improved due to better electrical conductivity and higher redox activity. Moreover, the honeycomb-like construction mitigates volumetric fluctuations while simultaneously providing enough area to temporarily hold polysulfide species. As shown in Figures 3I and 3J, the carbon-supported CoS₂ manifests a high initial discharge capacity of 1252.4 mAh g⁻¹ at 0.1 C and remarkable rate performance (754 mAh g⁻¹ at a high current rate of 4 C).

Carbon-supported dual-TMDs heterostructure

In the prior section, we mainly focus on the integration of a particular TMD with carbonaceous materials, which aims to harness their synergistic merits of conductivity from carbon and adsorptive/catalytic property of TMDs.³² Hopefully, the diversity of TMDs gives rise to various characteristics, so that dual-TMDs heterostructures could possess desirable properties to meet multiple demands with rational selection and integration.

Inspired by this, an advanced interlayer was proposed by Li et al. by anchoring a Co₉S₈@MoS₂ core-shell heterostructure to a carbon nanofiber (Co₉S₈@MoS₂/CNF) (Figure 4A).⁶⁸ Herein, the heterostructure incorporates the merits of high chemisorption of Co₉S₈ and good electrochemical catalytic capability of MoS₂. The calculated band structures of MoS₂, Co₉S₈, and Co₉S₈@MoS₂ are displayed in Figure 4B, which clearly suggest the improved metal characteristics of Co₉S₈@MoS₂ preserved from Co₉S₈. In addition, the tuned band structure of MoS₂ shell endows Co₉S₈@MoS₂/CNF strong adsorption to LiPSs and effective catalytic ability to convert LiPSs to Li₂S (Figures 4C and 4D).

To better reveal and visualize the improvement of sulfur electrochemistry at the molecular level and the dynamic anchoring-diffusion-transformation process of LiPSs, advanced characterization techniques have been valued. With this regard, the X-ray absorption near-edge structure (XANES) and extended X-ray absorption fine structure were utilized to further investigate the electronic structure and local coordination circumstance of samples (Figures 4E and 4F).⁶⁹ As shown in Figure 4G, both ZnS-SnS₂@NC and ZnS-SnS@NC heterostructures exhibit higher energy than SnS₂@NC and SnS@NC, suggesting strong electronic interactions across abundant interfaces. Similar results are observed in Figure 4H revealing the

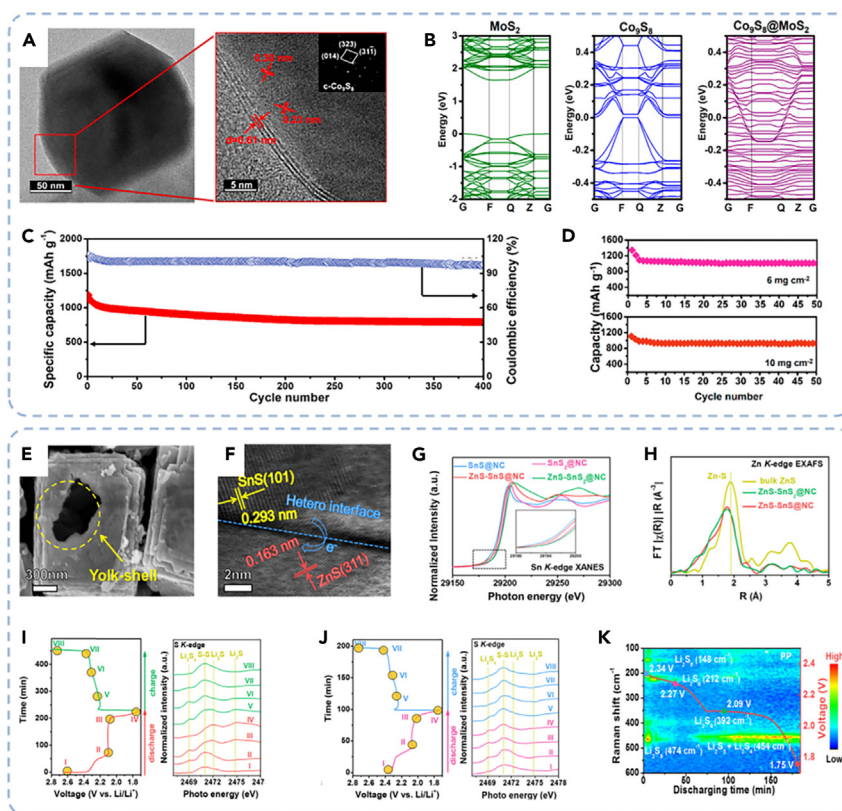


Figure 4. Carbon-supported dual-TMDs heterostructure in sulfur chemistry

(A) TEM and HRTEM images of MoS₂ layers.

(B) Projected band structures of MoS₂, Co₉S₈, and Co₉S₈@MoS₂.

(C) Long-term cycling performance of Li–S cells with Co₉S₈@MoS₂/CNF interlayer at 1 C with S loading of 3 mg cm⁻².

(D) Cycling performance of the Co₉S₈@MoS₂/CNF interlayer at 0.1 C with S loading of 6 and 10 mg cm⁻².⁶⁵ Copyright 2020, American Chemical Society.

(E and F) FE-SEM image and (F) HRTEM images of ZnS-SnS@NC.

(G) Sn K-edge XANES spectrum of the samples.

(H–J) Fourier transforms of Zn K-edge EXAFS spectrum of the samples. *ex situ* XANES of sulfur K-edge cathode for Li–S cells at various depths in the first discharge/charge process based on (I) ZnS-SnS@NC and (J) routine PP separator.

(K) *In situ* time-resolved Raman spectra obtained during the discharging processes with ZnS-SnS@NC modified separators.⁶⁹ Copyright 2021, American Chemical Society.

different local atomic arrangements between the materials. More significantly, *ex situ* XANES measurement of Li–S battery was performed to profoundly clarify the sulfur redox reaction mechanism. Of note, the strong peaks at 2471.0 eV and at 2472.0/2474.8 eV are attributed to S–S bonds of S₈ and Li₂S, respectively. Therefore, the gradual decreases and increased peaks demonstrate the transformation of S₈ to Li₂S and eventually converted to S₈ with the ZnS-SnS@NC during the whole discharge and charge process (Figure 4I). Compared to routine PP separator (Figure 4J), the distinguished change significantly illustrates the accelerated redox kinetics and highly reversible electrochemical process. In addition, the result of *in situ* Raman spectroscopy (Figure 4K) further testifies that ZnS-SnS@NC can efficiently impede shuttling of LiPSs.

Non-carbonaceous TMDs heterostructure

Apart from TMDs, new opportunities are receiving attention in numerous other polar metal compounds encompassing carbide, oxide, nitride, and MXene,^{70–73} which are applied to address these annoying issues in sulfur chemistry.

Nevertheless, a portion of the materials with too strong confinement to LiPSs would lead to the extinction of Li₂S_n species, resulting in an incomplete structure that would dissolve into the electrolyte.⁷⁴ For this

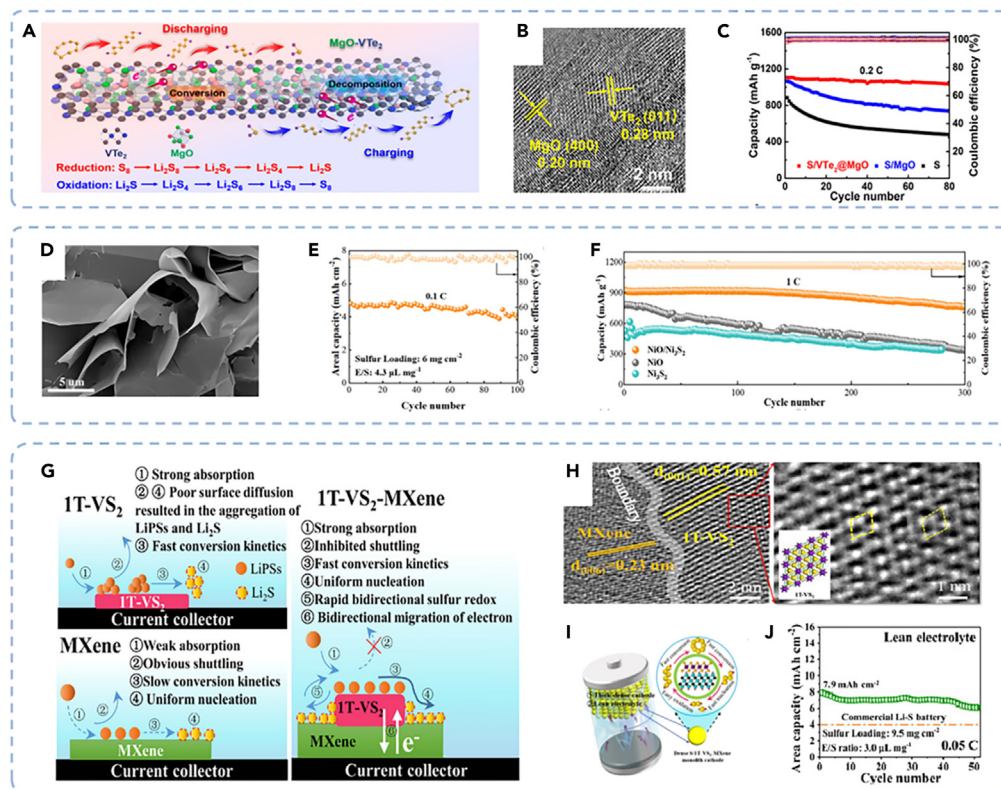


Figure 5. Non-carbonaceous TMDs heterostructure in sulfur chemistry

(A) Schematic of polysulfide regulation process by $\text{VTe}_2@\text{MgO}$ heterostructure.

(B) HRTEM image of $\text{VTe}_2@\text{MgO}$.

(C) Cycling performance of $\text{S}/\text{VTe}_2@\text{MgO}$, S/MgO , and S cathodes at 0.2 C.⁷⁵ Copyright 2019, American Chemical Society.

(D) SEM images of $\text{NiO}/\text{Ni}_3\text{S}_2$. (E) Rate performances and (F) long-term cycling performances of the $\text{NiO}/\text{Ni}_3\text{S}_2/\text{S}$, $\text{Ni}_3\text{S}_2/\text{S}$, and NiO/S electrodes.⁷⁶ Copyright 2022, Wiley-VCH.

(G) Schematic of the synergistic mechanism of $1\text{T-VS}_2\text{-MXene}$ heterostructure for the catalytic conversion and deposition of sulfur species.

(H) HRTEM images of $1\text{T-VS}_2\text{-MXene}$ heterostructure.

(I) Mechanism scheme of the compact Li-S with thick and dense $\text{S}/1\text{T-VS}_2\text{-MXene}$ monolith cathode.

(J) Areal capacities of thick dense $\text{S}/1\text{T-VS}_2\text{-MXene}$ monolith cathode at a low E/S ratio of 3.0 L mg^{-1} .⁷⁷ Copyright 2021, ELSEVIER B.V.

reason, the incorporation of transition metal dichalcogenides is an efficient resolvent by accelerating the redox kinetics simultaneously to enhance the utilization of sulfur. Wang et al. have controlled synthesis of electrically catalyzed $\text{VTe}_2@\text{MgO}$ heterostructures by atmospheric CVD, which is rarely realized by conventional wet chemical synthetic routes (Figure 5A).⁷⁵ The derived heterostructure strikes a balance between adsorption capability of MgO and catalytic activity of VTe_2 , resulting in harvesting favorable electrochemistry performances (Figures 5B and 5C).

Even more challenging from the perspective of practical application, most available heterostructures hardly match the criteria, especially with a high sulfur loading and lean electrolyte.⁷⁸ Recently, a topochemical conversion strategy by using $\text{Ni}(\text{OH})_2$ ultrathin nanosheets as a template was applied to develop non-layered $\text{NiO}/\text{Ni}_3\text{S}_2$ heterostructure nanosheets with ultrathin thickness (Figure 5D).⁷⁶ Benefiting from the ultrathin thickness and abundant exposed active sites, the obtained $\text{NiO}/\text{Ni}_3\text{S}_2$ cathode delivers an area capacity of 4.8 mAh cm^{-2} even under the high sulfur loading (6 mg cm^{-2}) and low electrolyte/sulfur ratio ($4.3 \text{ } \mu\text{L mg}^{-1}$) (Figure 5E). Moreover, the electrocatalyst stabilized at 920 mAh g^{-1} after 300 cycles (0.018% decay per cycle) at 1 C with this strategy extended to 2D Ni foil (Figure 5F). More recently, it is reported that Wu et al. developed a dual-conductive $1\text{T-VS}_2\text{-MXene}$ heterostructured electrocatalyst as a

high-efficiency sulfur host material (Figures 5G and 5H).⁷⁷ In contrast to 1T-VS₂ or MXene, the heterostructured catalyst integrates the advantages of ultrafast anchoring and catalysis (1T-VS₂) and excellent nucleation and surface diffusion (MXene), thereby acquiring a balanced bidirectional sulfur redox kinetics and ultimately obtaining improved electrochemical performance. Encouragingly, the highly dense S/1T-VS₂-MXene cathode obtains a desirable volumetric capacity with incorporating a dense sulfur monolith cathode design (Figure 5I). Even in such a hostile condition with lean electrolyte (3 $\mu\text{L mg}^{-1}$) and high sulfur loading (9.5 mg cm^{-2}), it still manifests a highly reversible specific capacity at 0.05 C with 77% capacity retention after 50 cycles (Figure 5J).

Defective TMDs

Apart from the introduction of other materials, defect engineering can effectively expose the active site and control the electron distribution of TMDs and further attain facile LiPSs conversion and stabilized sulfur chemistry.³³

Doping

It is well established that heteroatom doping facilitates material's electrocatalytic effect evoked by electronic modulation.^{79,80} Hence, the diversity of heteroatom provides wide opportunities for optimizing electric conductivity, electronic structure, and interface property of TMDs. As such, heteroatom doping has paved a broad way for suitable polysulfide mediators in the Li-S battery system, owing to the improved conductivity, polysulfide adsorption ability, and catalytic activity. The doped heteroatom typically encompasses two categories, metal heteroatoms (Fe, Co, Ni, etc.) and non-metal heteroatoms (N, O, B, P, etc.).

Metal heteroatom doping is believed to have a favorable impact on sulfur chemistry. In many cases, Co doping offers an enhanced promising catalyst for Li-S batteries to accelerate redox kinetic between polar surfaces.⁸⁰ Among the potential choices to relieve shuttle effect, SnS₂ has been proven to serve as an effective mediator for the adsorption and conversion of LiPSs.⁸¹ To further boost the potential of SnS₂, Gao et al. reported a Co-doped SnS₂ anchored on N-doped carbon nanotube as both a polysulfide barrier to relieve the impacts of shuttling effect and an electrocatalyst to enhance the kinetics of the conversion of LiPSs (Figure 6A).⁸² It reveals that Co doping provides an effective strategy for achieving high initial capacity and capacity retention for Li-S batteries (Figures 6B and 6C).

For non-metal doping, some recent works have revealed that optimized catalysts help strengthen interaction of TMDs with LiPSs. To deepen the understanding of LiPSs adsorption mechanism, Song et al. simulated the adsorption system of CoTe₂-N and CoTe₂, respectively, by DFT calculation.⁸⁵ As expected, CoTe₂-N shows evidently high binding energy with all sulfur species for that Li-N bond is more favorable to the anchoring of polysulfides than the Li-S bond. When S₈ is present, CoTe₂-N forms comparable Co-S bonds to CoTe₂ but stronger interaction with LiPSs. This inspiring result shows that N doping alters electron behavior in Co centers through the formation of Li-N bonds and enhanced Co-S interactions. In consequence, the superior lithophilicity and sulfiphilicity endow CoTe₂-N with improved LiPS management.

To investigate the underlying reason for increased chemical activity with N doping, Tian et al. studied the band structure of N-doping CoSe₂ (N-CoSe₂) and CoSe₂ through theoretical calculations.⁸³ Figure 6D shows that the *d*-band center of Co 3d in N-CoSe₂ clearly shifts to higher energy and appears to be closer to the Fermi level than CoSe₂. This demonstrates the higher charge density and advantageous charge transfer during sulfur redox processes with N-CoSe₂ catalyst. Moreover, according to the classical *d*-band center theory, the antibonding states are less filled when the closer the center of the *d*-band is to the Fermi level, which is prone to increase chemisorption with polysulfides. Therefore, N doping can not only strengthen the interaction with LiPSs but also reduce the activation energy of sulfur reduction processes (Figures 6E-G).

In fact, the co-doping technique was expected to produce greater interfacial interactions to trap polysulfides than single doping.⁸⁶ As far as we know, MoS₂ manifests strong confinement with LiPSs but their further application is often plagued by low conductivity and limited active sites. Along this line, simultaneous Co and P co-doping of MoS₂ is developed to improve its catalytic performance (Figures 6H and 6I).⁸⁴ Co doping is demonstrated to expedite the conversion of MoS₂ from 2H to metallic 1T phase, which is significant to raise the electrical conductivity and LiPSs affinity. At the same time, thus, derived Co-P

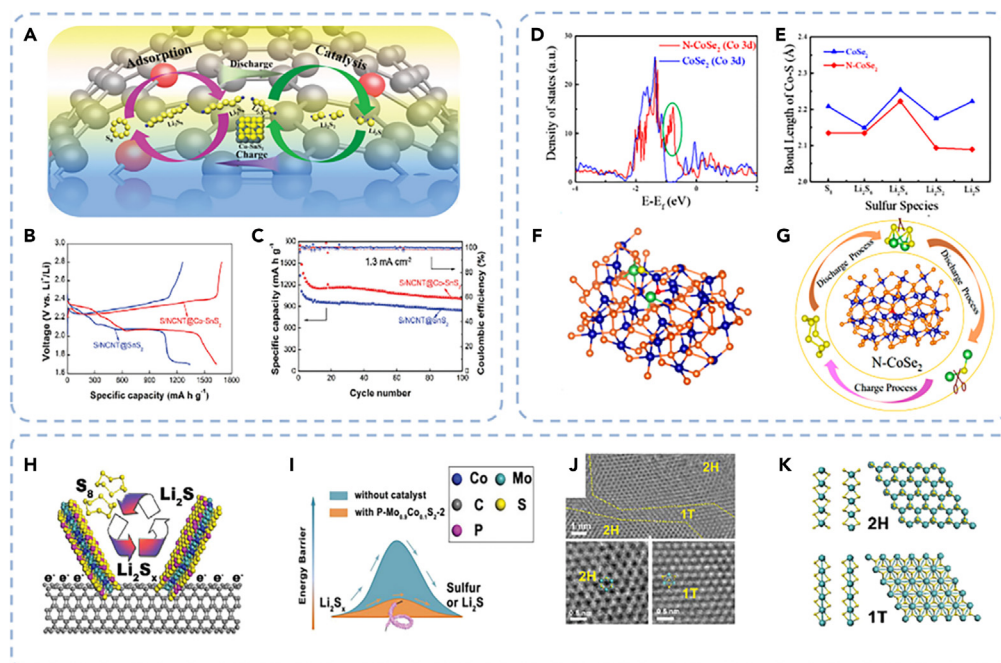


Figure 6. TMDs with heteroatom-doped TMDs in sulfur chemistry

(A) Schematic of polysulfide chemical regulation and catalytic conversion processes on S/NCNT@Co-SnS₂ electrode.

(B and C) CV profiles (second cycle) and (C) discharge/charge profiles of S/NCNT@SnS₂ and S/NCNT@Co-SnS₂ electrodes with an S loading of 3 mg cm⁻².⁸² Copyright 2019, Wiley-VCH.

(D) Calculated density of states of CoSe₂ and N-CoSe₂ with obvious shift of *d*-band in the green circle.

(E) Bond lengths of Co-S on the surface of CoSe₂ and N-CoSe₂.

(F) Decomposition model of Li₂S on the surface of N-CoSe₂.

(G) Schematic of possible conversion mechanism of S on the surface of N-CoSe₂.⁸³ Copyright 2020, American Chemical Society.

(H and I) Schematic of (H) conversion of Li₂S_x by P-Mo_{0.9}Co_{0.1}S₂ on CNT and (I) energy barrier in Li₂S_x conversion reactions with and without P-Mo_{0.9}Co_{0.1}S₂ catalyst.

(J) HRTEM images of Mo_{0.9}Co_{0.1}S₂.

(K) Schematic of the MoS₂ 2H and 1T structures.⁸⁴ Copyright 2019, Wiley-VCH.

coordinated sites exhibit high catalytic activity for LiPSs transformation. Consequently, the synergy effect of polysulfide confinement and catalyzed polysulfide conversion improves the electrochemical performance of Li-S batteries (Figures 6J and 6K).

Vacancy

Introducing vacancy to TMDs is another typical and efficient defect engineering technique, because of the enhanced conductivity and more acquired active sites for immobilization and conversion.^{87,88} With regards to TMDs, chalcogen vacancies and transition metal vacancies are two common categories.

Widely recognized, the polarity strength plays a major role in immobilizing the polar polysulfides, which apparently can be further increased by the generation of transition metal vacancy.⁷² For instance, Li et al. utilized one-step pyrolysis to *in situ* introduce Fe-vacancies into iron sulfide (Fe_{0.96}S) as sulfur host (Figure 7A).⁸⁹ Theoretical studies confirmed that the presence of Fe_{0.96}S crystal enhances electron mobility and Li⁺ diffusion (Figure 7B). Additionally, owing to the introduction of Fe-vacancies in FeS crystal, the adsorption capacity and catalytic effect for LiPSs have been significantly improved (Figure 7C).

Chalcogen vacancy has also demonstrated a remarkable potential for enhancing electrochemical activity by virtue of its distinct active sites and electronic characteristics.^{54,92} To this end, Ci et al. fabricated a defective VSe₂ combined with a vertically oriented graphene nanosheet on a carbon cloth by an all-CVD *in situ* built routine to serve as the sulfur host (Figure 7D).⁵⁸ In contrast to traditional wet chemistry method, the

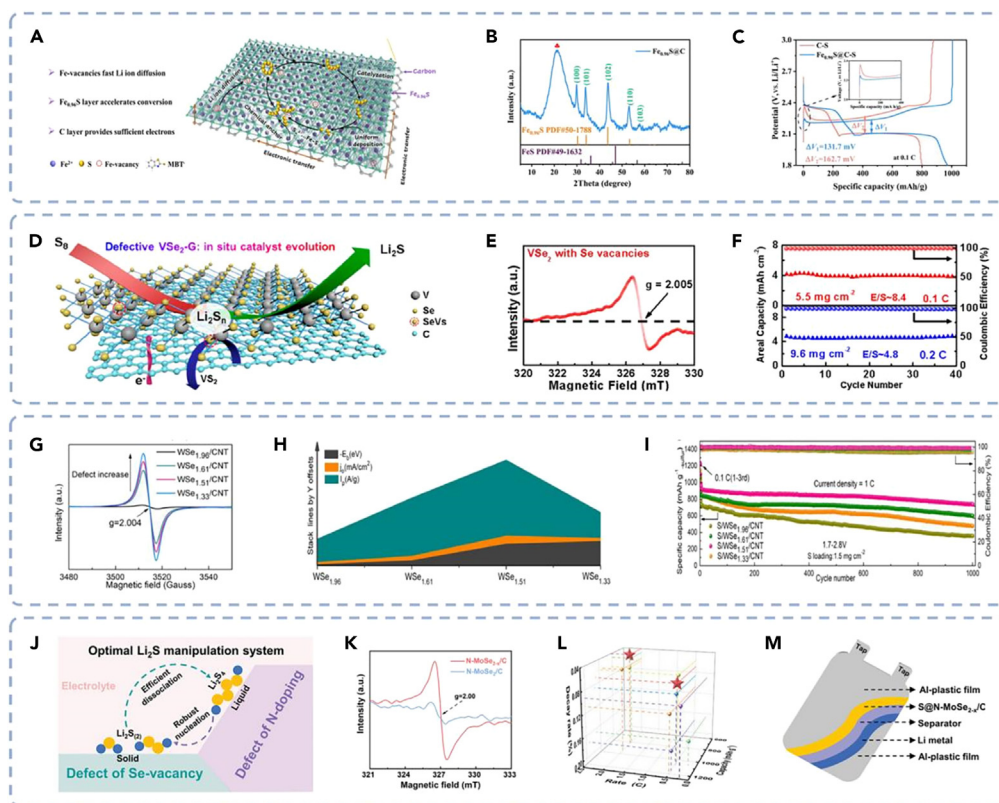


Figure 7. TMDs with vacancies in sulfur chemistry

- (A) Schematic of adsorption–conversion–conduction effect of $\text{Fe}_{0.96}\text{S}@C$ for LiPSs.
 (B) XRD patterns of $\text{Fe}_{0.96}\text{S}@C$.
 (C) Charge/discharge curves of $\text{Fe}_{0.96}\text{S}@C\text{-S}$ and C-S cathodes.⁸⁹ Copyright 2022, ELSEVIER B.V.
 (D) Schematic of discharge process at the $\text{SeVs-VSe}_2\text{-VG}@CC/S$ cathode.
 (E) EPR curve of VSe_2 .
 (F) Cycling performance of $\text{VSe}_2\text{-VG}@CC/S$ with elevated sulfur loadings. The unit of E/S ratio is $\mu\text{L mg}^{-1}$.⁵⁸ Copyright 2020, American Chemical Society.
 (G) EPR spectra of $\text{WSe}_{2-x}/\text{CNT}$.
 (H) Schematic of quantitative comparison of the electrochemical behavior of $\text{WSe}_{2-x}/\text{CNT}$.
 (I) Long-term cycling performances and Coulombic efficiency of $\text{WSe}_{2-x}/\text{CNT}$ at 1 C.⁹⁰ Copyright 2021, ELSEVIER B.V.
 (J) Schematic of the optimal Li_2S manipulation by selective dual-defect engineering with synergistic D_N and V_{Se} .
 (K) EPR spectra of $\text{N-MoSe}_{2-x}/\text{C}$ and $\text{N-MoSe}_2/\text{C}$.
 (L) Comparison of the electrochemical performance between $\text{S}@N\text{-MoSe}_{2-x}/\text{C}$ and other selenide-based cathodes for Li-S batteries.
 (M) Schematic of the flexible Li-S pouch cell with an $\text{S}@N\text{-MoSe}_{2-x}/\text{C}$ cathode.⁹¹ Copyright 2021, Wiley-VCH.

all-CVD approaches possess superior control of the interfacial engineering and defect manipulation (Figure 7E). Benefiting from the tight interface of heterostructure, catalytic activity of Se vacancy, and good electrical conductivity from metallic VSe_2 , the cathode harvests a distinguished high areal capacity of 4.9 mAh cm^{-2} even under a sulfur loading of 9.6 mg cm^{-2} (Figure 7F).

To shed light on the deep reasons for the influences of vacancy on catalytic performance, Li et al. quantitatively investigated the defective 2D WSe_2 with different W/Se ratios on enhancing the Li-S chemistry (Figure 7G).⁹⁰ Three fundamental parameters, the bonding energy E_b representing adsorption ability, the peak current intensity I_p in the CV representing diffusion barrier in the interface, and the exchange current j_0 representing catalytic ability are summarized for comparison in Figure 7H. Apparently, $\text{WSe}_{1.51}$ with a moderate level of defect retains the best performance for adsorbing polysulfides, catalyzing polysulfides conversion, and encouraging liquid-solid transformation (Figure 7I). These results give us some guides: on the one hand, the defect indeed not only has strong adsorption ability for LiPSs but also provides extra

catalytic sites for the conversion reactions of LiPSs. On the other hand, excessive defects can cause a decrease in confinement and catalytic ability owing to the transformation of defect site configuration. Hence, it is essential to reexamine the role of vacancy in Li–S system.

Moreover, tailored architecture with multiple defects offers a new opportunity to facilitate Li–S chemistry.⁹³ Shi et al. designed a unique dual-defect system (N-MoSe_{2-x}) to achieve synergism of the strong chemical adsorption and high electrocatalytic activity of electrode materials.⁹¹ In detail, N-doping and Se-vacancy selectively catalyze Li₂S nucleation and dissociation, accelerating bidirectional sulfur redox kinetics (Figures 7J and 7K). Through this well-designed dual-defect architecture, the uniform precipitation of Li₂S was achieved and the aggregation of LiPSs was inhibited. Considering the excellent bidirectional catalytic activity, the S@N-MoSe_{2-x}/C cathode manifested an outstanding reversible capacity and cyclic stability (Figure 7L). Notably, a flexible Li–S pouch cell using the S@N-MoSe_{2-x}/C cathode can likewise constantly energize an electronic device (Figure 7M).

Atom loading

Typically, the activity and selectivity of a given electrocatalyst are closely related to its electronic and geometric structures, which are dictated by particle size, interactions with the support/reactants, and potential phase evolution during catalytic reactions.⁹⁴ Considering the variety and complexity of catalytic processes, it seems necessary to visualize the relationship between the particle size of catalysts and their reactivity. Therefore, numerous efforts have been made with a large size distribution, including nanoparticles, nanoclusters, and single atoms. Among them, in the past few years, single-atom catalysts (SACs) made an astounding development in Li–S realm by virtue of the maximum atom utilization, tunable active sites, and remarkable electrochemistry stability.^{95,96} When SACs are dispersed on a TMDs substrate, the synergy of size effect and interface effect paves a way for further improvement of the catalytic performance.

Theoretical calculation has been considered a promising tool to predict the catalytic properties of SACs. In this sense, Nahian et al. contrasted the interaction of Li₂S_n on pristine and V@WSe₂ comprehensively, which included the sulfur reduction reactions and the catalytic decomposition of short-chain LiPSs by DFT simulation (Figures 8A–C).⁹⁷ Moreover, this study revealed the underlying mechanism of superior performance of V@WSe₂ by charge transfer, bond strength, and density of state analysis.

Along this way, Dong et al. eliminated traditional complex steps, distributing single Ni atoms on MoS₂ nanosheets via a facile injecting preparation method to modify separators of Li–S battery (Figure 8D).⁹⁸ The derived Ni-MoS₂ functional separator (Ni-MoS₂@PP) can adsorb polysulfides and accelerate the transformation of LiPSs due to the additional active catalytic sites obtained by introducing atomically distributed Ni species (Figures 8E and 8F). Consequently, the Li–S batteries exhibit fantastic electrochemical performance, including high initial capacity (599 mAh g⁻¹ at 2 C) and cycling stability (0.01% per cycle decay after 400 cycles at 2 C). When sulfur loading was increased to 7.5 mg cm⁻², it still retains a high areal capacity of 5.9 mAh cm⁻² after 50 cycles (Figures 8G and 8H).

APPLICATION OF TMDs IN LITHIUM ANODE

In lithium anode, uncontrollable dendrite growth has asserted possible risk of impaling separators and divorcing from the electrode, which would hamper the Coulombic efficiency and cycling stability of Li–S batteries.⁹⁹ In general, lithium dendrite growth entails a series of nucleation and plating/stripping processes. Because of the inhomogeneous nucleation, uneven interface should be formed, which would aggravate the growth of dendrites and further strengthen local electrical fields.¹⁰⁰

As mentioned before, numerous Li atoms can readily intercalate TMDs with the unique atomically layered structure. Hence, the space for Li diffusion is extended from the surface to each atomic interlayer,¹⁰¹ which significantly lowers the migration energy barrier, resulting in accelerated diffusion of Li⁺ and suppressed dendrite growth.¹⁰²

The addition of a protective layer between anode and separator has been proven to be effective in suppressing the formation and growth of harmful dendrites.^{103,104} For example, Cha et al. achieved a passivating Li anode by directly coating and lithiating an atomic 2D layer of MoS₂ onto the surface (Figures 9A and 9B).¹⁰⁵ Apart from the facilitated Li⁺ flux, they particularly discovered that the enhanced conductivity of the MoS₂ interlayer eliminated the preferential sites for Li dendrite nucleation. The obtained Li–S

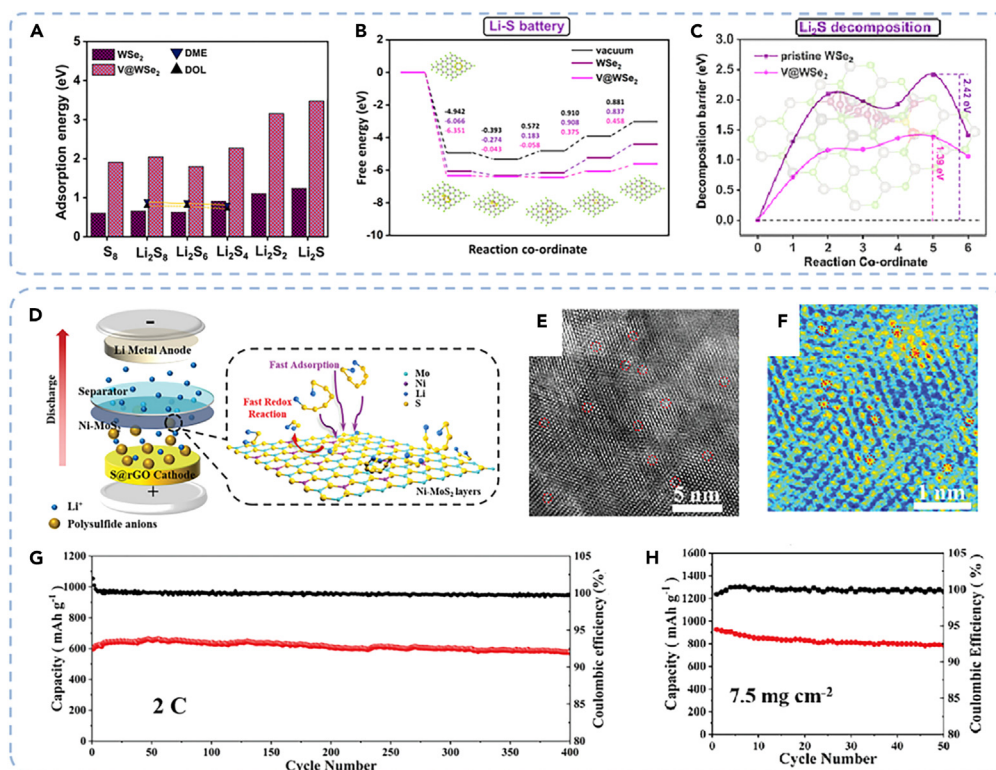


Figure 8. Single atom on TMDs in sulfur chemistry

- (A) Calculated adsorption energies of S_8 and Li_2S_n on both pristine and $V@WSe_2$.
 (B) Gibbs free energy profile of the SRR under vacuum and on pristine and $V@WSe_2$ for Li–S.
 (C) Computed decomposition barriers of Li_2S on $V@WSe_2$ substrates.⁹⁷ Copyright 2022, American Chemical Society.
 (D) Schematic of the working mechanism of Ni–MoS₂ nanosheets modified separator in Li–S battery.
 (E and F) Atomic resolution picture and (F) related FFT-filtered atomic resolution image of Ni–MoS₂ nanosheets.
 (G) Long-term performance of Ni–MoS₂@PP separator at 2 C.
 (H) Cycling performance of the Ni–MoS₂@PP separator with a high sulfur loading of 7.5 mg cm^{−2} at 0.2 C.⁹⁸ Copyright 2022, Wiley-VCH.

battery shows an outstanding Coulombic efficiency of ~98% for over 1200 cycles at 0.5 C (Figure 9C). More encouragingly, Wang et al. explored a facile integrated approach to prepare 2D hexagonal VS₂ flakes rather than conventional VS₂ microflowers (Figure 9D).¹⁰⁶ Given the enhanced stable hexagonal multilayered nanostructure, the protective layer not only homogenizes Li deposition but also resists the lithium dendrite growth physically by improving the puncture resistance of PP separator (Figures 9E–H).

In addition to focusing on exterior remediation (separator modification or interlayer insertion), well-designed 3D conductive matrix is also effective in further stabilizing Li anode.^{107–109} He et al. designed a flexible and free-standing framework by integrating catalytic and lithiophilic 1T'-MoTe₂ nanosheets with conductive carbon nanotubes (MoTe₂-CNT) (Figure 9I).⁵⁹ When serving as a host for both sulfur cathode and lithium anode, the Li–S full cell established a remarkable electrochemical performance. Notably, MoTe₂-CNT not only induced the homogeneous growth of Li within the framework but also created a thin SEI consisting of lithium telluride (Figures 9J–L). The sulfide-rich SEI further stabilized Li deposition and prolonged cycle life of the system, which indicated attraction of the transition metal telluride as a host of Li anode.

CONCLUSIONS AND OUTLOOK

In summary, we systematically discuss and highlight the application of 2D TMDs in Li–S batteries reported in recent years. In this contribution, the unique property and synthetic strategy of TMDs have been firstly introduced. Based on the extensive experimental and theoretical research, special attention is paid to

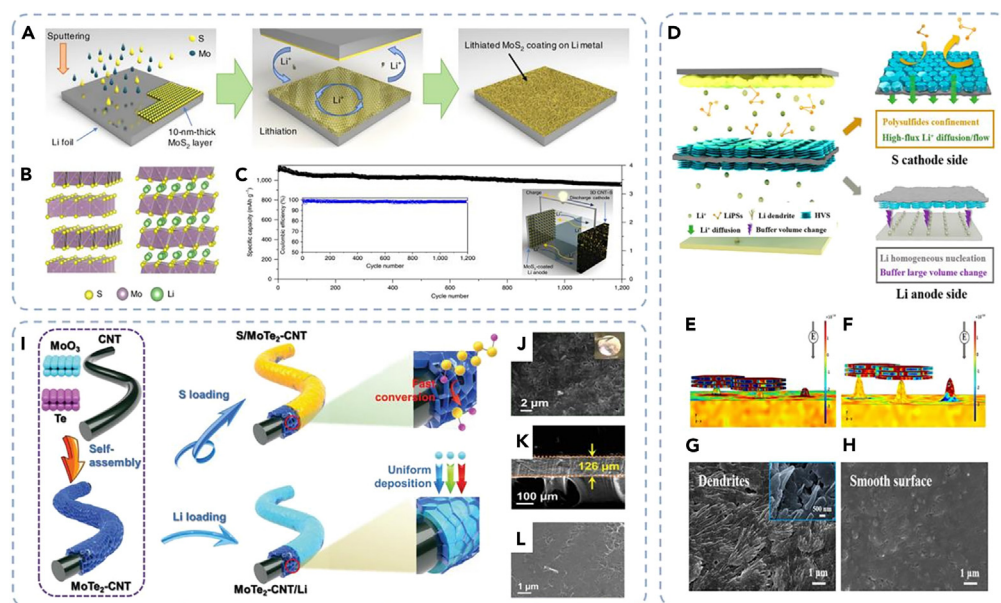


Figure 9. TMDs in lithium anode

(A) Schematic of the preparation of MoS₂-coated Li metal.

(B) Model structures of pristine 2H-MoS₂ and 1T Li-MoS₂.

(C) Long-term cycling performance of Li-S battery with the 3D CNT-S cathode and the MoS₂-coated Li anode at 0.5 C.¹⁰⁵ Copyright 2018, Springer Nature Limited.

(D) Schematic of the working principle of the Li-S battery with PP and D-HVS@PP separator.

(E and F) COMSOL Multiphysics simulation of the electric field distribution at different growth periods of the lithium dendrites covered with the HVS layer.

(G and H) SEM images of the lithium metal anodes with (G) PP and (H) D-HVS@PP separators after stripping/plating for 100 cycles.¹⁰⁶ Copyright 2020, American Chemical Society.

(I) Schematic of the synthesis route for S/MoTe₂-CNT and MoTe₂-CNT/Li. (J) Top-surface and (K) cross-sectional morphologies of MoTe₂-CNT/Li. (L) SEM image of Li anode extracted from S/MoTe₂-CNT||MoTe₂-CNT/Li cells after 50 cycles.⁵⁹ Copyright 2021, Wiley-VCH.

three main types (pristine TMDs, TMD composite, and defective TMDs). Further efforts have been devoted to revealing the underlying mechanism of TMDs in accelerating sulfur chemistry and stabilizing lithium anode. Undoubtedly, TMDs display promising potential as a versatile component for Li-S batteries, including host, catalyst, adsorbent, and protective layer (Tables 1 and 2), by virtue of various chemical compositions, tunable band structures, and distinctive electronic structures.

Despite these encouraging advances, there are still considerable opportunities to fully utilize the properties of TMDs in Li-S realm. Hence, special attention should be paid to the following aspects (Figure 10).

- (1) Controllable synthesis: In the third section, the commonly employed preparation routes of TMDs in EES devices, including CVD, hydro(solvo)thermal synthesis, and exfoliation, have shown their pros and cons, respectively. Therefore, it is significantly important to ameliorate the current synthesis process or explore emerging approaches to strike a balance between product quality and cost efficiency. More challenging, the preparation of TMDs with properties in a controllable manner remains a formidable hurdle. Notably, nowadays, some novel strategies extend the possibilities for producing 2D TMDs such as molecular beam epitaxy and atomic layer deposition.^{111,112}
- (2) Rational modulation: 2D TMDs are rising as promising candidates for Li-S batteries because of the outstanding LiPS confinement, catalytic capability, and lithiophilicity. Despite the 2D TMDs are focused as promising candidate for Li-S batteries, ongoing works are still needed to further improve their electrochemical performance for the limited exposed active sites and unsatisfied conductivity. Several engineering strategies have been established to deal with the issues that pristine TMDs faced, pertaining to hybrid engineering, defect engineering, and band engineering. Among

Table 1. Summary of various TMDs employed in boosting sulfur chemistry

TMDs classification	Materials	Sulfur loading [mg cm ⁻²]	Capacity at low current [mAh g ⁻¹]	Capacity at high current [mAh g ⁻¹]	Cycle (rate)/Decay rate [%]	Reference
Pristine TMDs	WS ₂	–	700 (0.2 C)	–	350 (0.5 C)/0.025	Babu et al. ²⁹
	MoS ₂	–	1471 (0.1 C)	550 (1 C)	600 (0.5 C)/0.083	Ghazi et al. ¹¹⁰
TMDs composites	ReS ₂ @CNT	6.5	1360 (0.1 C)	839 (2 C)	1000 (1 C)/0.028	He et al. ⁵⁵
	V-MoS ₂ /rGOCTF	4.0–6.0	1379 (0.1 C)	530 (5 C)	500 (0.1 C)/0.028	Cui et al. ⁵⁶
	GC–CoS ₂	2.5	1252 (0.1 C)	687 (4 C)	1000 (2 C)/0.032	Liu et al. ⁵⁷
	Co ₉ S ₈ @MoS ₂ /CNF	3.0	1221 (0.1 C)	477 (5 C)	400 (1 C)/0.091	Li et al. ⁶⁸
	ZnS-SnS@NC	2.0–2.2	1349 (0.2 C)	706 (8 C)	2000 (4 C)/0.013	Yao et al. ⁶⁹
	VTe ₂ @MgO	1.4–1.6	1107 (0.2 C)	705 (3 C)	1000 (1 C)/0.055	Wang et al. ⁷⁵
	NiO/Ni ₃ S ₂	1.1	1580 (0.1 C)	640 (2 C)	300 (1 C)/0.018	Jin et al. ⁷⁶
	1T-VS ₂ –MXene	1.2	1379 (0.1 C)	517 (5 C)	500 (1 C)/0.079	Wu et al. ⁷⁷
Defective TMDs	NCNT@Co-SnS ₂	3.0	1337 (0.2 C)	–	300 (0.5 C)/0.16	Gao et al. ⁸²
	N-CoSe ₂	2.0	1632 (0.05 C)	926 (2 C)	500 (2 C)/0.037	Wang et al. ⁸³
	P-Mo _{0.9} Co _{0.1} S ₂	2.0	1485 (0.2 C)	931 (6 C)	600 (1 C)/0.046	Lin et al. ⁸⁴
	Fe _{0.96} S@C	1.8	809 (0.5 C)	420 (5 C)	400 (1 C)/0.018	Li et al. ⁸⁹
	SeVs-MoSe ₂	–	1348 (0.2 C)	784 (3 C)	400 (2 C)/0.050	Wang et al. ⁵⁴
	VSe ₂ –VG@CC	1.4–1.7	1480 (0.2 C)	450 (5 C)	800 (5 C)/0.039	Ci et al. ⁵⁸
	WSe _{1.51}	1.5	1346 (0.05 C)	839 (2 C)	1000 (1 C)/0.025	Li et al. ⁹⁰
	N-MoSe _{2-x} /C	1.5	1141 (0.2 C)	637 (3 C)	1000 (2 C)/0.040	Shi et al. ⁹¹
Ni-MoS ₂	2.5	1329 (0.2 C)	677 (3 C)	400 (2 C)/0.009	Dong et al. ⁹⁸	

them, hybrid engineering has the advantages of friendliness to novices and obvious effect. It must be pointed out that *d*-band center theory ensures us probe and understand the origin of improved LiPS adsorption and catalytic activity for LiPS conversion. The unoccupied *d*-band of transition metal is considered active site for catalysis. By this way, rational upshift of *d*-band centers renders material higher confinement of LiPSs and lower reaction energy barrier, thus leading to enhanced redox kinetics. Additionally, two or more strategies are indispensable in some cases and further broaden application scenarios. For example, the criticized issues of inert catalytic activity and low electrical conductivity can be resolved simultaneously by designing a carbon-support N-doping MoS₂.

- (3) Precise characterization: On one hand, many engineering tactics have been developed to enhance the characteristics of TMDs. Consequently, accurate characterization of targeted material confirms completely the transformation of phase of TMDs. On the other hand, understanding the mechanisms of TMDs in Li–S realm should not be ignored. Several *in situ* characterization techniques provide powerful tools for comprehensive real-time exploration of these mechanisms and properties, including Raman spectroscopy, X-ray diffraction, transmission electron microscope, ultraviolet-visible spectroscopy, XANES, and atomic force microscope. These advanced characterizations help reveal and visualize dynamic anchoring-diffusion-transformation process of LiPSs. In this case, breakthroughs of *in situ* methods such as nuclear magnetic resonance¹¹³ will result in cutting-edge research in the field of Li–S battery.

Table 2. Summary of various TMDs employed in protecting lithium anode

TMDs classification	Materials	Performance	Reference
Pristine TMDs	MoS ₂	~52 mV voltage polarization at 10 mA cm ⁻² after 300 cycles	Xu et al. ¹⁰⁵
TMDs composites	MoTe ₂ -CNT	6 mAh cm ⁻² (1800h) at 6 mA cm ⁻²	Heet al. ⁵⁹
	D-HVS	0.5 mAh cm ⁻² (400h) at 5 mA cm ⁻²	Wang et al. ¹⁰⁶
	ZnSe-CoSe ₂ @NC	3 mAh cm ⁻² (1000h) at 3 mA cm ⁻²	Xu et al., ¹⁰⁸
	CoTe= NCGs	2 mAh cm ⁻² (900h) at 2 mA cm ⁻²	Li et al. ¹⁰⁹

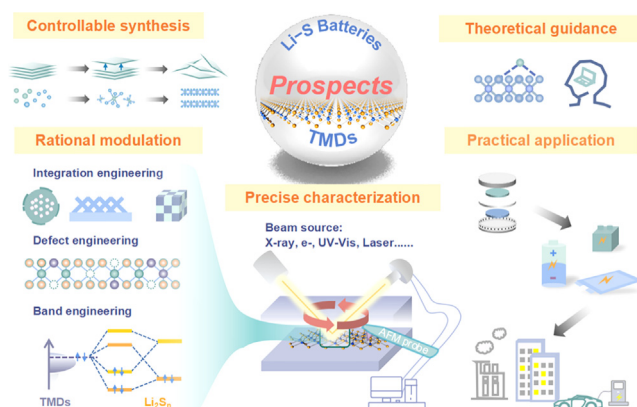


Figure 10. Promising endeavors of TMDs for Li-S batteries

- (4) Theoretical guidance: DFT simulation and machine learning method have played an important role in guiding the development of ideal materials. Considering the variety of TMDs, theoretical calculations will help to screen candidates efficiently by comparing specific parameters (e.g., adsorption configurations and adsorption energies of Li_2S_x , d -band center of the catalyst, and electric field distribution at different growth periods). Moreover, theoretical guidance assists to analysis potential electronic structure, atomic configurations, and the catalytic pathway.
- (5) Practical application: At present, realizing a high energy density Li-S battery becomes the primary mission because the ultimate purpose of Li-S battery is to serve production and life. As cell size and operating environment complexity continue to increase, the factors affecting TMDs commercialization need to be further studied. Therefore, great attention should be paid to electrochemical performance under harsh testing conditions of high sulfur loading, lean electrolyte, and low lithium consumption.

Limitations of the study

It should be noted that this review emphasized only representative development and application of 2D TMDs in expediting sulfur chemistry and stabilizing lithium anode in Li-S batteries, without any discussion for electrolyte designing. In addition, regarding most of reported electrochemical performances based on inconsistent testing conditions, more parameters need to be considered to adapt to different application scenarios.

ACKNOWLEDGMENTS

This work was supported by the National Natural Science Foundation of China (22179089) and Undergraduate Training Program for Innovation and Entrepreneurship, Soochow University (202210285031Z). The authors acknowledge the support from Suzhou Key Laboratory for Advanced Carbon Materials and Wearable Energy Technologies, Suzhou, China.

AUTHOR CONTRIBUTIONS

Conceptualization: X.Y., Y.D., and J.S. Investigation, interpretation, and compilation: X.Y. and Y.D. Visualization: X.Y. and Y.D. Supervision: J.S. Writing-Original Draft: X.Y. and Y.D. Writing-Review and Editing: X.Y., Y.D., and J.S.

DECLARATION OF INTERESTS

The authors declare no competing interests.

INCLUSION AND DIVERSITY

We support inclusive, diverse, and equitable conduct of research.

REFERENCES

- Evers, S., and Nazar, L.F. (2013). New approaches for high energy density lithium–sulfur battery cathodes. *Acc. Chem. Res.* **46**, 1135–1143. <https://doi.org/10.1021/ar3001348>.
- Chen, Z.X., Zhao, M., Hou, L.P., Zhang, X.Q., Li, B.Q., and Huang, J.Q. (2022). Toward Practical High-Energy-Density Lithium–Sulfur Pouch Cells: A Review. *Adv. Mater.* **34**, 2201555. <https://doi.org/10.1002/adma.202201555>.
- Service, R.F. (2018). Lithium-sulfur batteries poised for leap. *Science* **359**, 1080–1081. <https://doi.org/10.1126/science.359.6380.1080>.
- Seh, Z.W., Sun, Y., Zhang, Q., and Cui, Y. (2016). Designing high-energy lithium-sulfur batteries. *Chem. Soc. Rev.* **45**, 5605–5634. <https://doi.org/10.1039/c5cs00410a>.
- Bruce, P.G., Freunberger, S.A., Hardwick, L.J., and Tarascon, J.M. (2011). Li–O₂ and Li–S batteries with high energy storage. *Nat. Mater.* **11**, 19–29. <https://doi.org/10.1038/nmat3191>.
- Lei, J., Liu, T., Chen, J., Zheng, M., Zhang, Q., Mao, B., and Dong, Q. (2020). Exploring and understanding the roles of Li₂S_n and the strategies to beyond present Li–S batteries. *Chem* **6**, 2533–2557. <https://doi.org/10.1016/j.chempr.2020.06.032>.
- Manthiram, A., Fu, Y., Chung, S.H., Zu, C., and Su, Y.S. (2014). Rechargeable lithium-sulfur batteries. *Chem. Rev.* **114**, 11751–11787. <https://doi.org/10.1021/cr500062v>.
- Bhargava, A., He, J., Gupta, A., and Manthiram, A. (2020). Lithium-sulfur batteries: attaining the critical metrics. *Joule* **4**, 285–291. <https://doi.org/10.1016/j.joule.2020.01.001>.
- Liu, Y.-z., Wang, Y., Wang, C.-w., Wang, J.-y., and Wang, J.-z. (2020). Recent advances in graphene materials used in Li–S batteries. *Carbon* **167**, 930–1011. <https://doi.org/10.1016/j.carbon.2020.04.046>.
- Deng, D.-R., Bai, C.-D., Xue, F., Lei, J., Xu, P., Zheng, M.-S., and Dong, Q.-F. (2019). Multifunctional ion-sieve constructed by 2D materials as an interlayer for Li–S batteries. *ACS Appl. Mater. Interfaces* **11**, 11474–11480. <https://doi.org/10.1021/acsami.8b22660>.
- Hou, J., Wang, Y., Yang, W., Wang, F., Yang, D., Zhang, Y., Liang, F., Li, X., Zhang, Y., and Zhao, J. (2022). Application of MXenes in lithium-sulfur batteries. *Sci. China Technol. Sci.* **65**, 2259–2273. <https://doi.org/10.1007/s11431-021-2077-5>.
- Yun, Q., Li, L., Hu, Z., Lu, Q., Chen, B., and Zhang, H. (2020). Layered Transition Metal Dichalcogenide-Based Nanomaterials for Electrochemical Energy Storage. *Adv. Mater.* **32**, 1903826. <https://doi.org/10.1002/adma.201903826>.
- Gao, Y.-P., Wu, X., Huang, K.-J., Xing, L.-L., Zhang, Y.-Y., and Liu, L. (2017). Two-dimensional transition metal diseleniums for energy storage application: a review of recent developments. *CrystEngComm* **19**, 404–418. <https://doi.org/10.1039/c6ce02223e>.
- Sun, L., Liu, Y., Xie, J., Fan, L., Wu, J., Jiang, R., and Jin, Z. (2023). Polar Co9S8 anchored on Pyrrole-Modified graphene with *in situ* growth of CNTs as multifunctional Self-Supporting medium for efficient Lithium–Sulfur batteries. *Chem. Eng. J.* **451**, 138370. <https://doi.org/10.1016/j.cej.2022.138370>.
- Yang, R., Mei, L., Zhang, Q., Fan, Y., Shin, H.S., Voiry, D., and Zeng, Z. (2022). High-yield production of mono- or few-layer transition metal dichalcogenide nanosheets by an electrochemical lithium ion intercalation-based exfoliation method. *Nat. Protoc.* **17**, 358–377. <https://doi.org/10.1038/s41596-021-00643-w>.
- Ma, L., Hendrickson, K.E., Wei, S., and Archer, L.A. (2015). Nanomaterials: Science and applications in the lithium–sulfur battery. *Nano Today* **10**, 315–338. <https://doi.org/10.1016/j.nantod.2015.04.011>.
- Zhou, L., Danilov, D.L., Eichel, R.A., and Notten, P.H.L. (2020). Host materials anchoring polysulfides in Li–S batteries reviewed. *Adv. Energy Mater.* **11**, 2001304. <https://doi.org/10.1002/aenm.202001304>.
- Xie, J., Song, Y.W., Li, B.Q., Peng, H.J., Huang, J.Q., and Zhang, Q. (2020). Direct intermediate regulation enabled by sulfur containers in working lithium-sulfur batteries. *Angew. Chem. Int. Ed.* **59**, 22150–22155. <https://doi.org/10.1002/anie.202008911>.
- Abraham, A.M., Boteju, T., Ponnurangam, S., and Thangadurai, V. (2022). A global design principle for polysulfide electrocatalysis in lithium-sulfur batteries—A computational perspective. *Battery Energy J.* **20220003**. <https://doi.org/10.1002/bte2.20220003>.
- Shen, Z., Cao, M., Zhang, Z., Pu, J., Zhong, C., Li, J., Ma, H., Li, F., Zhu, J., Pan, F., and Zhang, H. (2019). Efficient Ni₂Co₄P₃ nanowires catalysts enhance ultrahigh-loading lithium-sulfur conversion in a microreactor-like battery. *Adv. Funct. Mater.* **30**, 1906661. <https://doi.org/10.1002/adfm.201906661>.
- Lv, R., Robinson, J.A., Schaak, R.E., Sun, D., Sun, Y., Mallouk, T.E., and Terrones, M. (2015). Transition metal dichalcogenides and beyond: synthesis, properties, and applications of single- and few-layer nanosheets. *Acc. Chem. Res.* **48**, 56–64. <https://doi.org/10.1021/ar5002846>.
- Dong, C., Gao, W., Jin, B., and Jiang, Q. (2018). Advances in Cathode Materials for High-Performance Lithium–Sulfur Batteries. *iScience* **6**, 151–198. <https://doi.org/10.1016/j.isci.2018.07.021>.
- Tan, C., and Zhang, H. (2015). Two-dimensional transition metal dichalcogenide nanosheet-based composites. *Chem. Soc. Rev.* **44**, 2713–2731. <https://doi.org/10.1039/c4cs00182f>.
- Zhang, Y., Zhang, L., Lv, T., Chu, P.K., and Huo, K. (2020). Two-dimensional transition metal chalcogenides for alkali metal ions storage. *ChemSusChem* **13**, 1114–1154. <https://doi.org/10.1002/cssc.201903245>.
- Wang, J., Yang, S., Xu, Z., Ai, G., Zhang, T., and Mao, W. (2022). Addressing the Prominent Li⁺ Intercalation Process of Metal Sulfide Catalyst in Li–S Batteries. *Adv. Mater. Interfaces* **9**, 2101699. <https://doi.org/10.1002/admi.202101699>.
- Xue, W., Shi, Z., Suo, L., Wang, C., Wang, Z., Wang, H., So, K.P., Maurano, A., Yu, D., Chen, Y., et al. (2019). Intercalation-conversion hybrid cathodes enabling Li–S full-cell architectures with jointly superior gravimetric and volumetric energy densities. *Nat. Energy* **4**, 374–382. <https://doi.org/10.1038/s41560-019-0351-0>.
- Chen, Y., Lai, Z., Zhang, X., Fan, Z., He, Q., Tan, C., and Zhang, H. (2020). Phase engineering of nanomaterials. *Nat. Rev. Chem* **4**, 243–256. <https://doi.org/10.1038/s41570-020-0173-4>.
- Kang, K., Xie, S., Huang, L., Han, Y., Huang, P.Y., Mak, K.F., Kim, C.J., Muller, D., and Park, J. (2015). High-mobility three-atom-thick semiconducting films with wafer-scale homogeneity. *Nature* **520**, 656–660. <https://doi.org/10.1038/nature14417>.
- Babu, G., Masurkar, N., Al Salem, H., and Arava, L.M.R. (2017). Transition Metal Dichalcogenide Atomic Layers for Lithium Polysulfides Electrocatalysis. *J. Am. Chem. Soc.* **139**, 171–178. <https://doi.org/10.1021/jacs.6b08681>.
- Chhowalla, M., Shin, H.S., Eda, G., Li, L.J., Loh, K.P., and Zhang, H. (2013). The chemistry of two-dimensional layered transition metal dichalcogenide nanosheets. *Nat. Chem.* **5**, 263–275. <https://doi.org/10.1038/nchem.1589>.
- Shen, Z., Zhang, Z., Li, M., Yuan, Y., Zhao, Y., Zhang, S., Zhong, C., Zhu, J., Lu, J., and Zhang, H. (2020). Rational design of a Ni₃N_{0.85} electrocatalyst to accelerate polysulfide conversion in lithium-sulfur batteries. *ACS Nano* **14**, 6673–6682. <https://doi.org/10.1021/acsnano.9b09371>.
- Huang, S., Wang, Z., Von Lim, Y., Wang, Y., Li, Y., Zhang, D., and Yang, H.Y. (2021). Recent advances in heterostructure engineering for lithium-sulfur batteries. *Adv. Energy Mater.* **11**, 2003689. <https://doi.org/10.1002/aenm.202003689>.
- Shi, Z., Li, M., Sun, J., and Chen, Z. (2021). Defect engineering for expediting Li–S chemistry: strategies, mechanisms, and perspectives. *Adv. Energy Mater.* **11**, 2100332. <https://doi.org/10.1002/aenm.202100332>.
- Truong, Q.D., Kempaiah Devaraju, M., Nakayasu, Y., Tamura, N., Sasaki, Y., Tomai, T., and Honma, I. (2017). Exfoliated MoS₂

- and MoSe₂ nanosheets by a supercritical fluid process for a hybrid Mg-Li-ion battery. *ACS Omega* 2, 2360–2367. <https://doi.org/10.1021/acsomega.7b00379>.
35. Zhou, J., Wang, L., Yang, M., Wu, J., Chen, F., Huang, W., Han, N., Ye, H., Zhao, F., Li, Y., and Li, Y. (2017). Hierarchical VS₂ nanosheet assemblies: a universal host material for the reversible storage of alkali metal ions. *Adv. Mater.* 29, 1702509. <https://doi.org/10.1002/adma.201702061>.
 36. Tan, C., Luo, Z., Chaturvedi, A., Cai, Y., Du, Y., Gong, Y., Huang, Y., Lai, Z., Zhang, X., Zheng, L., et al. (2018). Preparation of High-Percentage 1T-Phase Transition Metal Dichalcogenide Nanodots for Electrochemical Hydrogen Evolution. *Adv. Mater.* 30, 1705509. <https://doi.org/10.1002/adma.201705509>.
 37. Chhowalla, M., Liu, Z., and Zhang, H. (2015). Two-dimensional transition metal dichalcogenide (TMD) nanosheets. *Chem. Soc. Rev.* 44, 2584–2586. <https://doi.org/10.1039/C5CS90037A>.
 38. Zheng, J., Yan, X., Lu, Z., Qiu, H., Xu, G., Zhou, X., Wang, P., Pan, X., Liu, K., and Jiao, L. (2017). High-mobility multilayered MoS₂ flakes with low contact resistance grown by chemical vapor deposition. *Adv. Mater.* 29, 1604540. <https://doi.org/10.1002/adma.201604540>.
 39. Matte, H.S.S.R., Gomathi, A., Manna, A.K., Late, D.J., Datta, R., Pati, S.K., and Rao, C.N.R. (2010). MoS₂ and WS₂ analogues of graphene. *Angew. Chem. Int. Ed.* 49, 4059–4062. <https://doi.org/10.1002/anie.201000009>.
 40. Coleman, J.N., Lotya, M., O'Neill, A., Bergin, S.D., King, P.J., Khan, U., Young, K., Gaucher, A., De, S., Smith, R.J., et al. (2011). Two-dimensional nanosheets produced by liquid exfoliation of layered materials. *Science* 331, 568–571. <https://doi.org/10.1126/science.1194975>.
 41. Zhou, J., Lin, J., Huang, X., Zhou, Y., Chen, Y., Xia, J., Wang, H., Xie, Y., Yu, H., Lei, J., et al. (2018). A library of atomically thin metal chalcogenides. *Nature* 556, 355–359. <https://doi.org/10.1038/s41586-018-0008-3>.
 42. Zhou, J., Zhu, C., Zhou, Y., Dong, J., Li, P., Zhang, Z., Wang, Z., Lin, Y.-C., Shi, J., Zhang, R., et al. (2023). Composition and phase engineering of metal chalcogenides and phosphorous chalcogenides. *Nat. Mater.* 22, 450–458. <https://doi.org/10.1038/s41563-022-01291-5>.
 43. Sun, L., Yuan, G., Gao, L., Yang, J., Chhowalla, M., Gharahcheshmeh, M.H., Gleason, K.K., Choi, Y.S., Hong, B.H., and Liu, Z. (2021). Chemical vapour deposition. *Nat. Rev. Methods Primers* 1, 5. <https://doi.org/10.1038/s43586-020-00005-y>.
 44. Xu, J., Zhang, J., Zhang, W., and Lee, C.-S. (2017). Interlayer nanoarchitectonics of two-dimensional transition-metal dichalcogenides nanosheets for energy storage and conversion applications. *Adv. Energy Mater.* 7, 1700571. <https://doi.org/10.1002/aenm.201700571>.
 45. Krishnamoorthy, K., Veerasubramani, G.K., Radhakrishnan, S., and Kim, S.J. (2014). Supercapacitive properties of hydrothermally synthesized sphere like MoS₂ nanostructures. *Mater. Res. Bull.* 50, 499–502. <https://doi.org/10.1016/j.materresbull.2013.11.019>.
 46. Chen, Y.M., Yu, X.Y., Li, Z., Paik, U., and Lou, X.W.D. (2016). Hierarchical MoS₂ tubular structures internally wired by carbon nanotubes as a highly stable anode material for lithium-ion batteries. *Sci. Adv.* 2, e1600021. <https://doi.org/10.1126/sciadv.1600021>.
 47. Geng, H., Yang, J., Dai, Z., Zhang, Y., Zheng, Y., Yu, H., Wang, H., Luo, Z., Guo, Y., Zhang, Y., et al. (2017). Co₉S₈/MoS₂ yolk-shell spheres for advanced Li/Na storage. *Small* 13, 1603490. <https://doi.org/10.1002/sml.201603490>.
 48. Chung, S.H., and Manthiram, A. (2017). Lithium–sulfur batteries with the lowest self-discharge and the longest shelf life. *ACS Energy Lett.* 2, 1056–1061. <https://doi.org/10.1021/acseenergylett.7b00245>.
 49. Li, T., Bai, X., Gulzar, U., Bai, Y.-J., Capiglia, C., Deng, W., Zhou, X., Liu, Z., Feng, Z., and Proietti Zaccaria, R. (2019). A comprehensive understanding of lithium–sulfur battery technology. *Adv. Funct. Mater.* 29, 1901730. <https://doi.org/10.1002/adfm.201901730>.
 50. Yang, Y., Zheng, G., and Cui, Y. (2013). Nanostructured sulfur cathodes. *Chem. Soc. Rev.* 42, 3018–3032. <https://doi.org/10.1039/C2CS35256G>.
 51. Wang, H., Yang, Y., Liang, Y., Robinson, J.T., Li, Y., Jackson, A., Cui, Y., and Dai, H. (2011). Graphene-wrapped sulfur particles as a rechargeable lithium–sulfur battery cathode material with high capacity and cycling stability. *Nano Lett.* 11, 2644–2647. <https://doi.org/10.1021/nl200658a>.
 52. Ji, X., Lee, K.T., and Nazar, L.F. (2009). A highly ordered nanostructured carbon–sulphur cathode for lithium–sulphur batteries. *Nat. Mater.* 8, 500–506. <https://doi.org/10.1038/nmat2460>.
 53. Liu, X., Huang, J.-Q., Zhang, Q., and Mai, L. (2017). Nanostructured metal oxides and sulfides for lithium–sulfur batteries. *Adv. Mater.* 29, 1601759. <https://doi.org/10.1002/adma.201601759>.
 54. Wang, M., Sun, Z., Ci, H., Shi, Z., Shen, L., Wei, C., Ding, Y., Yang, X., and Sun, J. (2021). Identifying the evolution of selenium-vacancy-modulated MoSe₂ pre-catalyst in lithium-sulfur chemistry. *Angew. Chem. Int. Ed.* 60, 24558–24565. <https://doi.org/10.1002/anie.202109291>.
 55. He, J., Bhargava, A., Yaghoobnejad Asl, H., Chen, Y., and Manthiram, A. (2020). 1T'-ReS₂ nanosheets *in situ* grown on carbon nanotubes as a highly efficient polysulfide electrocatalyst for stable Li-S Batteries. *Adv. Energy Mater.* 10, 2001017. <https://doi.org/10.1002/aenm.202001017>.
 56. Cui, B., Cai, X., Wang, W., Saha, P., and Wang, G. (2022). Nano storage-boxes constructed by the vertical growth of MoS₂ on graphene for high-performance Li-S batteries. *J. Energy Chem.* 66, 91–99. <https://doi.org/10.1016/j.jechem.2021.06.035>.
 57. Liu, J., Xiao, S.H., Zhang, Z., Chen, Y., Xiang, Y., Liu, X., Chen, J.S., and Chen, P. (2020). Naturally derived honeycomb-like N,S-codoped hierarchical porous carbon with MS₂ (M = Co, Ni) decoration for high-performance Li-S battery. *Nanoscale* 12, 5114–5124. <https://doi.org/10.1039/c9nr10419d>.
 58. Ci, H., Cai, J., Ma, H., Shi, Z., Cui, G., Wang, M., Jin, J., Wei, N., Lu, C., Zhao, W., et al. (2020). Defective VSe₂-graphene heterostructures enabling *in situ* electrocatalyst evolution for lithium-sulfur batteries. *ACS Nano* 14, 11929–11938. <https://doi.org/10.1021/acsnano.0c05030>.
 59. He, J., Bhargava, A., and Manthiram, A. (2021). *In situ* grown 1T'-MoTe₂ nanosheets on carbon nanotubes as an efficient electrocatalyst and lithium regulator for stable lithium–sulfur full cells. *Adv. Energy Mater.* 12, 2103204. <https://doi.org/10.1002/aenm.202103204>.
 60. Bhojate, S., Kim, J., Lee, E., Park, B., Lee, E., Park, J., Oh, S.H., Kim, J., and Choi, W. (2020). Mixed phase 2D Mo_{0.5}W_{0.5}S₂ alloy as a multi-functional electrocatalyst for a high-performance cathode in Li-S batteries. *J. Mater. Chem.* 8, 12436–12445. <https://doi.org/10.1039/d0ta04354k>.
 61. Yang, Z., Hu, Z., Yan, G., Li, M., Feng, Y., Qu, X., and Zhang, X. (2022). Multi-function hollow nanorod as an efficient sulfur host accelerates sulfur redox reactions for high-performance Li-S batteries. *J. Colloid Interface Sci.* 629, 65–75. <https://doi.org/10.1016/j.jcis.2022.09.015>.
 62. Gao, J., Li, L., Tan, J., Sun, H., Li, B., Idrobo, J.C., Singh, C.V., Lu, T.-M., and Koratkar, N. (2016). Vertically Oriented Arrays of ReS₂ Nanosheets for Electrochemical Energy Storage and Electrocatalysis. *Nano Lett.* 16, 3780–3787. <https://doi.org/10.1021/acs.nanolett.6b01180>.
 63. Cheng, Z., Chen, Y., Yang, Y., Zhang, L., Pan, H., Fan, X., Xiang, S., and Zhang, Z. (2021). Metallic MoS₂ nanoflowers decorated graphene nanosheet catalytically boosts the volumetric capacity and cycle life of lithium–sulfur batteries. *Adv. Energy Mater.* 11, 2003718. <https://doi.org/10.1002/aenm.202003718>.
 64. Zhang, X.Q., Cui, Y.L., Zhong, Y., Wang, D.H., Tang, W.J., Wang, X.L., Xia, X.H., Gu, C.D., and Tu, J.P. (2019). Cobalt disulfide-modified cellular hierarchical porous carbon derived from bovine bone for application in high-performance lithium–sulfur batteries. *J. Colloid Interface Sci.* 551, 219–226. <https://doi.org/10.1016/j.jcis.2019.04.079>.
 65. Paraknowitsch, J.P., and Thomas, A. (2013). Doping carbons beyond nitrogen: an overview of advanced heteroatom doped carbons with boron, sulphur and phosphorus for energy applications. *Energy*

- Environ. Sci. 6, 2839–2855. <https://doi.org/10.1039/c3ee41444b>.
66. Tang, C., Zhang, Q., Zhao, M.Q., Huang, J.Q., Cheng, X.B., Tian, G.L., Peng, H.J., and Wei, F. (2014). Nitrogen-doped aligned carbon nanotube/graphene sandwiches: facile catalytic growth on bifunctional natural catalysts and their applications as scaffolds for high-rate lithium-sulfur batteries. *Adv. Mater.* 26, 6100–6105. <https://doi.org/10.1002/adma.201401243>.
67. Wang, J., and Han, W.-Q. (2022). A review of heteroatom doped materials for advanced lithium-sulfur batteries. *Adv. Funct. Mater.* 32, 2107166. <https://doi.org/10.1002/adfm.202107166>.
68. Li, B., Su, Q., Yu, L., Zhang, J., Du, G., Wang, D., Han, D., Zhang, M., Ding, S., and Xu, B. (2020). Tuning the band structure of MoS₂ via Co₉S₈@MoS₂ core-shell structure to boost catalytic activity for lithium-sulfur batteries. *ACS Nano* 14, 17285–17294. <https://doi.org/10.1021/acsnano.0c07332>.
69. Yao, W., Zheng, W., Xu, J., Tian, C., Han, K., Sun, W., and Xiao, S. (2021). ZnS-SnS@NC heterostructure as robust lithiophilicity and sulfiphilicity mediator toward high-rate and long-life lithium-sulfur batteries. *ACS Nano* 15, 7114–7130. <https://doi.org/10.1021/acsnano.1c00270>.
70. Ding, Y., Shi, Z., Sun, Y., Wu, J., Pan, X., and Sun, J. (2023). Steering bidirectional sulfur redox via geometric/electronic mediator comodulation for Li-S batteries. *ACS Nano* 17, 6002–6010. <https://doi.org/10.1021/acsnano.3c00377>.
71. Qiao, Z., Zhang, Y., Meng, Z., Xie, Q., Lin, L., Zheng, H., Sa, B., Lin, J., Wang, L., and Peng, D.-L. (2021). Anchoring polysulfides and accelerating redox reaction enabled by Fe-based compounds in lithium-sulfur batteries. *Adv. Funct. Mater.* 31, 2100970. <https://doi.org/10.1002/adfm.202100970>.
72. Wang, H., Zhang, W., Xu, J., and Guo, Z. (2018). Advances in polar materials for lithium-sulfur batteries. *Adv. Funct. Mater.* 28, 1707520. <https://doi.org/10.1002/adfm.201707520>.
73. Shafique, A., Vanhulsel, A., Rangasamy, V.S., Baert, K., Hauffman, T., Adriaensens, P., Safari, M., Van Bael, M.K., Hardy, A., and Sallard, S. (2023). DBD Plasma-Assisted Coating of Metal Alkoxides on Sulfur Powder for Li-S Batteries (*Battery Energy n/a*), 20220053. <https://doi.org/10.1002/bte2.20220053>.
74. Yuan, C., Song, X., Zeng, P., Liu, G., Zhou, S., Zhao, G., Li, H., Yan, T., Mao, J., Yang, H., et al. (2023). Precisely optimizing polysulfides adsorption and conversion by local coordination engineering for high-performance Li-S batteries. *Nano Energy* 110, 108353. <https://doi.org/10.1016/j.nanoen.2023.108353>.
75. Wang, M., Song, Y., Sun, Z., Shao, Y., Wei, C., Xia, Z., Tian, Z., Liu, Z., and Sun, J. (2019). Conductive and catalytic VTe₂@MgO heterostructure as effective polysulfide promoter for lithium-sulfur batteries. *ACS Nano* 13, 13235–13243. <https://doi.org/10.1021/acsnano.9b06267>.
76. Jin, C., Zhai, P., Tang, J., Huo, L., He, Q., Ye, Y., Qiu, L., Jiang, K., Shang, L., Li, Y., et al. (2023). Ultrathin NiO/Ni₃S₂ heterostructure as electrocatalyst for accelerated polysulfide conversion in lithium-sulfur batteries. *Energy Environ. Mater.* 0, e12491. <https://doi.org/10.1002/eem2.12491>.
77. Wu, S., Wang, W., Shan, J., Wang, X., Lu, D., Zhu, J., Liu, Z., Yue, L., and Li, Y. (2022). Conductive 1T-VS₂-MXene heterostructured bidirectional electrocatalyst enabling compact Li-S batteries with high volumetric and areal capacity. *Energy Storage Mater.* 49, 153–163. <https://doi.org/10.1016/j.ensm.2022.04.004>.
78. Yu, B., Huang, A., Srinivas, K., Zhang, X., Ma, F., Wang, X., Chen, D., Wang, B., Zhang, W., Wang, Z., et al. (2021). Outstanding catalytic effects of 1T'-MoTe₂ quantum dots@3D graphene in shuttle-free Li-S batteries. *ACS Nano* 15, 13279–13288. <https://doi.org/10.1021/acsnano.1c03011>.
79. Ge, W., Wang, L., Li, C., Wang, C., Wang, D., Qian, Y., and Xu, L. (2020). Conductive cobalt doped niobium nitride porous spheres as an efficient polysulfide converter for advanced lithium-sulfur batteries. *J. Mater. Chem.* 8, 6276–6282. <https://doi.org/10.1039/D0TA00800A>.
80. Zhang, J., Shi, Y., Ding, Y., Peng, L., Zhang, W., and Yu, G. (2017). A conductive molecular framework derived Li₂S/N,P-codoped carbon cathode for advanced lithium-sulfur batteries. *Adv. Energy Mater.* 7, 1602876. <https://doi.org/10.1002/aenm.201602876>.
81. Luo, L., Chung, S.-H., and Manthiram, A. (2018). A three-dimensional self-assembled SnS₂-nano-dots@graphene hybrid aerogel as an efficient polysulfide reservoir for high-performance lithium-sulfur batteries. *J. Mater. Chem.* 6, 7659–7667. <https://doi.org/10.1039/c8ta01089g>.
82. Gao, X., Yang, X., Li, M., Sun, Q., Liang, J., Luo, J., Wang, J., Li, W., Liang, J., Liu, Y., et al. (2019). Cobalt-doped SnS₂ with dual active centers of synergistic absorption-catalysis effect for high-S loading Li-S batteries. *Adv. Funct. Mater.* 29, 1806724. <https://doi.org/10.1002/adfm.201806724>.
83. Wang, M., Fan, L., Sun, X., Guan, B., Jiang, B., Wu, X., Tian, D., Sun, K., Qiu, Y., Yin, X., et al. (2020). Nitrogen-doped CoSe₂ as a bifunctional catalyst for high areal capacity and lean electrolyte of Li-S battery. *ACS Energy Lett.* 5, 3041–3050. <https://doi.org/10.1021/acsenenergylett.0c01564>.
84. Lin, H., Zhang, S., Zhang, T., Ye, H., Yao, Q., Zheng, G.W., and Lee, J.Y. (2019). Simultaneous cobalt and phosphorous doping of MoS₂ for improved catalytic performance on polysulfide conversion in lithium-sulfur batteries. *Adv. Energy Mater.* 9, 1902096. <https://doi.org/10.1002/aenm.201902096>.
85. Song, X., Tian, D., Qiu, Y., Sun, X., Jiang, B., Zhao, C., Zhang, Y., Xu, X., Fan, L., and Zhang, N. (2021). Efficient polysulfide trapping and conversion on N-Doped CoTe₂ via enhanced dual-anchoring effect. *Small* 17, 2102962. <https://doi.org/10.1002/smlf.202102962>.
86. Wu, H., Xia, L., Ren, J., Zheng, Q., Xu, C., and Lin, D. (2017). A high-efficiency N/P co-doped graphene/CNT@porous carbon hybrid matrix as a cathode host for high performance lithium-sulfur batteries. *J. Mater. Chem.* 5, 20458–20472. <https://doi.org/10.1039/C7TA06504C>.
87. Liu, X., Zhao, L., Xu, H., Huang, Q., Wang, Y., Hou, C., Hou, Y., Wang, J., Dang, F., and Zhang, J. (2020). Tunable cationic vacancies of cobalt oxides for efficient electrocatalysis in Li-O₂ batteries. *Adv. Energy Mater.* 10, 2001415. <https://doi.org/10.1002/aenm.202001415>.
88. Chao, D., Zhou, W., Ye, C., Zhang, Q., Chen, Y., Gu, L., Davey, K., and Qiao, S.-Z. (2019). An electrolytic Zn-MnO₂ battery for high-voltage and scalable energy storage. *Angew. Chem. Int. Ed.* 58, 7823–7828. <https://doi.org/10.1002/anie.201904174>.
89. Li, R., Sun, H., Chang, C., Yao, Y., Pu, X., and Mai, W. (2022). *In situ* induced cation-vacancies in metal sulfides as dynamic electrocatalyst accelerating polysulfides conversion for Li-S battery. *J. Energy Chem.* 75, 74–82. <https://doi.org/10.1016/j.jechem.2022.08.015>.
90. Li, H.-J., Xi, K., Wang, W., Liu, S., Li, G.-R., and Gao, X.-P. (2022). Quantitatively regulating defects of 2D tungsten selenide to enhance catalytic ability for polysulfide conversion in a lithium sulfur battery. *Energy Storage Mater.* 45, 1229–1237. <https://doi.org/10.1016/j.ensm.2021.11.024>.
91. Shi, Z., Sun, Z., Cai, J., Yang, X., Wei, C., Wang, M., Ding, Y., and Sun, J. (2021). Manipulating electrocatalytic Li₂S redox via selective dual-defect engineering for Li-S batteries. *Adv. Mater.* 33, 2103050. <https://doi.org/10.1002/adma.202103050>.
92. Zeng, P., Zhou, Z., Li, B., Yu, H., Zhou, X., Chen, G., Chang, B., Chen, M., Shu, H., Su, J., and Wang, X. (2022). Insight into the catalytic role of defect-enriched vanadium sulfide for regulating the adsorption-catalytic conversion behavior of polysulfides in Li-S batteries. *ACS Appl. Mater. Interfaces* 14, 35833–35843. <https://doi.org/10.1021/acsnami.2c09791>.
93. Song, H., Li, T., He, T., Wang, Z., Fang, D., Wang, Y., Li, X.L., Zhang, D., Hu, J., and Huang, S. (2022). Cooperative catalytic Mo-S-Co heterojunctions with sulfur vacancies for kinetically boosted lithium-sulfur battery. *Chem. Eng. J.* 450, 138115. <https://doi.org/10.1016/j.cej.2022.138115>.
94. Xiang, J., Shen, W., Guo, Z., Meng, J., Yuan, L., Zhang, Y., Cheng, Z., Shen, Y., Lu, X., and Huang, Y. (2021). A supramolecular complex of C₆₀-S with high-density active sites as a cathode for lithium-sulfur batteries. *Angew. Chem. Int. Ed.* 60, 14313–14318. <https://doi.org/10.1002/anie.202016247>.

95. Ding, Y., Cheng, Q., Wu, J., Yan, T., Shi, Z., Wang, M., Yang, D., Wang, P., Zhang, L., and Sun, J. (2022). Enhanced dual-directional sulfur redox via a biotemplated single-atomic Fe–N₂ mediator promises durable Li–S batteries. *Adv. Mater.* **34**, 2202256. <https://doi.org/10.1002/adma.202202256>.
96. Huang, T., Sun, Y., Wu, J., Shi, Z., Ding, Y., Wang, M., Su, C., Li, Y.-y., and Sun, J. (2022). Altering local chemistry of single-atom coordination boosts bidirectional polysulfide conversion of Li–S batteries. *Adv. Funct. Mater.* **32**, 2203902. <https://doi.org/10.1002/adfm.202203902>.
97. Nahian, M.S., Jayan, R., and Islam, M.M. (2022). Atomic-scale insights into comparative mechanisms and kinetics of Na–S and Li–S batteries. *ACS Catal.* **12**, 7664–7676. <https://doi.org/10.1021/acscatal.2c01174>.
98. Dong, C., Zhou, C., Li, Y., Yu, Y., Zhao, T., Zhang, G., Chen, X., Yan, K., Mai, L., and Xu, X. (2023). Ni single atoms on MoS₂ nanosheets enabling enhanced kinetics of Li–S batteries. *Small* **19**, 2205855. <https://doi.org/10.1002/smll.202205855>.
99. Zuo, T.-T., Wu, X.-W., Yang, C.-P., Yin, Y.-X., Ye, H., Li, N.-W., and Guo, Y.-G. (2017). Graphitized carbon fibers as multifunctional 3D current collectors for high areal capacity Li anodes. *Adv. Mater.* **29**, 1700389. <https://doi.org/10.1002/adma.201700389>.
100. Li, S., Huang, J., Cui, Y., Liu, S., Chen, Z., Huang, W., Li, C., Liu, R., Fu, R., and Wu, D. (2022). A robust all-organic protective layer towards ultrahigh-rate and large-capacity Li metal anodes. *Nat. Nanotechnol.* **17**, 613–621. <https://doi.org/10.1038/s41565-022-01107-2>.
101. Chen, B., Chao, D., Liu, E., Jaroniec, M., Zhao, N., and Qiao, S.-Z. (2020). Transition metal dichalcogenides for alkali metal ion batteries: engineering strategies at the atomic level. *Energy Environ. Sci.* **13**, 1096–1131. <https://doi.org/10.1039/c9ee03549d>.
102. Wang, L., Zhang, Q., Zhu, J., Duan, X., Xu, Z., Liu, Y., Yang, H., and Lu, B. (2019). Nature of extra capacity in MoS₂ electrodes: Molybdenum atoms accommodate with lithium. *Energy Storage Mater.* **16**, 37–45. <https://doi.org/10.1016/j.ensm.2018.04.025>.
103. Zhang, C., Fei, B., Yang, D., Zhan, H., Wang, J., Diao, J., Li, J., Henkelman, G., Cai, D., Biendicho, J.J., et al. (2022). Robust lithium-sulfur batteries enabled by highly conductive WSe₂-based superlattices with tunable interlayer space. *Adv. Funct. Mater.* **32**, 2201322. <https://doi.org/10.1002/adfm.202201322>.
104. Fan, L., Li, M., Li, X., Xiao, W., Chen, Z., and Lu, J. (2019). Interlayer material selection for lithium-sulfur batteries. *Joule* **3**, 361–386. <https://doi.org/10.1016/j.joule.2019.01.003>.
105. Cha, E., Patel, M.D., Park, J., Hwang, J., Prasad, V., Cho, K., and Choi, W. (2018). 2D MoS₂ as an efficient protective layer for lithium metal anodes in high-performance Li–S batteries. *Nat. Nanotechnol.* **13**, 337–344. <https://doi.org/10.1038/s41565-018-0061-y>.
106. Wang, J., Yi, S., Liu, J., Sun, S., Liu, Y., Yang, D., Xi, K., Gao, G., Abdelkader, A., Yan, W., et al. (2020). Suppressing the shuttle effect and dendrite growth in lithium-sulfur batteries. *ACS Nano* **14**, 9819–9831. <https://doi.org/10.1021/acsnano.0c02241>.
107. Wang, T.-S., Liu, X., Wang, Y., and Fan, L.-Z. (2021). High areal capacity dendrite-free Li anode enabled by metal-organic framework-derived nanorod array modified carbon cloth for solid state Li metal batteries. *Adv. Funct. Mater.* **31**, 2001973. <https://doi.org/10.1002/adfm.202001973>.
108. Xu, J., Xu, L., Zhang, Z., Sun, B., Jin, Y., Jin, Q., Liu, H., Wang, G., Liang, S., Guo, J.G., et al. (2022). Heterostructure ZnSe–CoSe₂ embedded with yolk-shell conductive dodecahedral as Two-in-one hosts for cathode and anode protection of Lithium–Sulfur full batteries. *Energy Storage Mater.* **47**, 223–234. <https://doi.org/10.1016/j.ensm.2022.02.010>.
109. Li, B., Wang, P., Xi, B., Song, N., An, X., Chen, W., Feng, J., and Xiong, S. (2022). In-situ embedding CoTe catalyst into 1D–2D nitrogen-doped carbon to didirectionally regulate lithium–sulfur batteries. *Nano Res.* **15**, 8972–8982. <https://doi.org/10.1007/s12274-022-4537-6>.
110. Ghazi, Z.A., He, X., Khattak, A.M., Khan, N.A., Liang, B., Iqbal, A., Wang, J., Sin, H., Li, L., and Tang, Z. (2017). MoS₂/Celgard separator as efficient polysulfide barrier for long-life lithium-sulfur batteries. *Adv. Mater.* **29**, 1606817. <https://doi.org/10.1002/adma.201606817>.
111. Li, H., Wu, J., Yin, Z., and Zhang, H. (2014). Preparation and applications of mechanically exfoliated single-layer and multi layer MoS₂ and WSe₂ nanosheets. *Acc. Chem. Res.* **47**, 1067–1075. <https://doi.org/10.1021/ar4002312>.
112. Yue, R., Barton, A.T., Zhu, H., Azcatl, A., Pena, L.F., Wang, J., Peng, X., Lu, N., Cheng, L., Addou, R., et al. (2015). HfSe₂ thin films: 2D transition metal dichalcogenides grown by molecular beam epitaxy. *ACS Nano* **9**, 474–480. <https://doi.org/10.1021/nn5056496>.
113. Simon, P., and Gogotsi, Y. (2013). Capacitive Energy Storage in Nanostructured Carbon-Electrolyte Systems. *Acc. Chem. Res.* **46**, 1094–1103. <https://doi.org/10.1021/ar200306b>.